Article

Cell Reports

Adaptive Thermogenesis in Mice Is Enhanced by Opsin 3-Dependent Adipocyte Light Sensing

Graphical Abstract

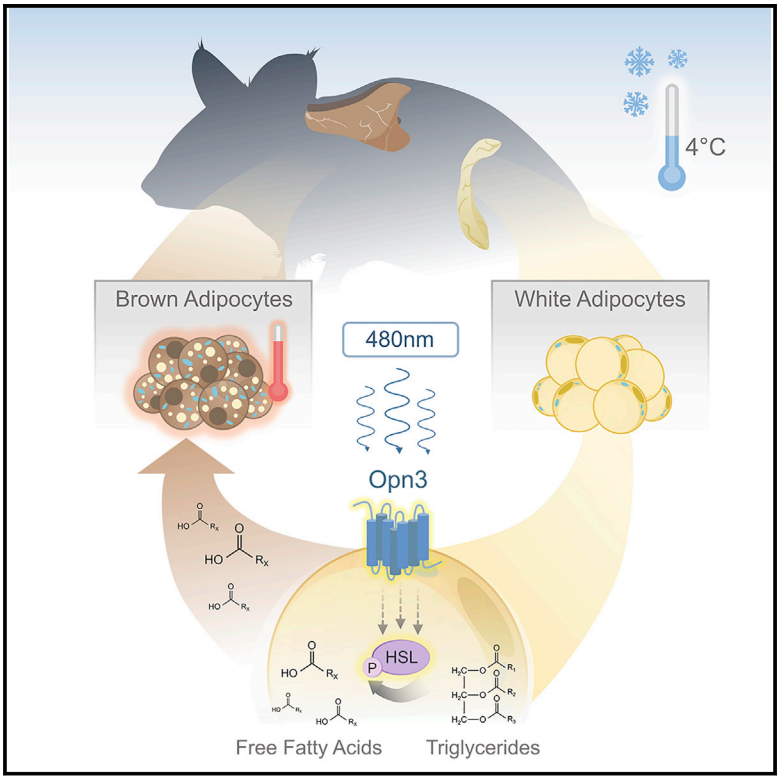

Authors

Gowri Nayak, Kevin X. Zhang, Shruti Vemaraju, ..., Russell N. Van Gelder, Joan Sanchez-Gurmaches, Richard A. Lang

Correspondence

richard.lang@cchmc.org

In Brief

White adipocytes activate the lipolysis pathway to produce the free fatty acids that are used as heating fuel by brown adipose tissue. Nayak et al. show that Opsin 3 is required for blue-light-enhanced activation of the lipolysis pathway. This explains the low body temperature of *Opn3* mutant mice.

Highlights

- Adipocytes express encephalopsin (OPN3), a 480 nm blue-light-sensitive opsin
- Mice lacking OPN3 or blue light have diminished thermogenesis during cold exposure
- Loss of OPN3 reduces oxygen consumption and energy expenditure
- White adipocyte OPN3 promotes lipolysis during cold exposure

Nayak et al., 2020, Cell Reports *30*, 672–686
January 21, 2020
https://doi.org/10.1016/j.celrep.2019.12.043

CellPress

OPEN ACCESS
CellPress

Cell Reports
Article

Adaptive Thermogenesis in Mice Is Enhanced by Opsin 3-Dependent Adipocyte Light Sensing

Gowri Nayak,[1,2,16] Kevin X. Zhang,[1,2,16] Shruti Vemaraju,[1,2,16] Yoshinobu Odaka,[1,2] Ethan D. Buhr,[9] Amanda Holt-Jones,[14] Stace Kernodle,[15] April N. Smith,[1,2] Brian A. Upton,[1,2] Shane D'Souza,[1,2] Jesse J. Zhan,[1,2] Nicolás Diaz,[9] Minh-Thanh Nguyen,[1,2] Rajib Mukherjee,[4] Shannon A. Gordon,[9] Gang Wu,[1,6] Robert Schmidt,[1,6] Xue Mei,[1,2] Nathan T. Petts,[5] Matthew Batie,[5] Sujata Rao,[12] John B. Hogenesch,[1,6] Takahisa Nakamura,[3,4,8,13] Alison Sweeney,[14] Randy J. Seeley,[15] Russell N. Van Gelder,[9,10,11] Joan Sanchez-Gurmaches,[3,4,8] and Richard A. Lang[1,2,3,7,17,*]

[1]Center for Chronobiology, Cincinnati Children's Hospital Medical Center, Cincinnati, OH 45229, USA
[2]The Visual Systems Group, Abrahamson Pediatric Eye Institute, Division of Pediatric Ophthalmology, Cincinnati Children's Hospital Medical Center, Cincinnati, OH 45229, USA
[3]Division of Developmental Biology, Cincinnati Children's Hospital Medical Center, Cincinnati, OH 45229, USA
[4]Division of Endocrinology, Cincinnati Children's Hospital Medical Center, Cincinnati, OH 45229, USA
[5]Division of Clinical Engineering, Cincinnati Children's Hospital Medical Center, Cincinnati, OH 45229, USA
[6]Division of Human Genetics, Cincinnati Children's Hospital Medical Center, Cincinnati, OH 45229, USA
[7]Department of Ophthalmology, University of Cincinnati, College of Medicine, Cincinnati, OH 45267, USA
[8]Department of Pediatrics, University of Cincinnati, College of Medicine, Cincinnati, OH 45267, USA
[9]Department of Ophthalmology, University of Washington Medical School, Seattle, WA 98104, USA
[10]Department of Biological Structure, University of Washington Medical School, Seattle, WA 98104, USA
[11]Department of Pathology, University of Washington Medical School, Seattle, WA 98104, USA
[12]The Cleveland Clinic, Ophthalmic Research, 9500 Euclid Avenue, OH 44195, USA
[13]Department of Metabolic Bioregulation, Institute of Development, Aging and Cancer, Tohoku University, Sendai, Miyagi 980-8575, Japan
[14]Department of Physics and Astronomy, University of Pennsylvania, Philadelphia, PA 19104, USA
[15]Department of Surgery, University of Michigan, Ann Arbor, MI 48109, USA
[16]These authors contributed equally
[17]Lead Contact
*Correspondence: richard.lang@cchmc.org
https://doi.org/10.1016/j.celrep.2019.12.043

SUMMARY

Almost all life forms can detect and decode light information for adaptive advantage. Examples include the visual system, in which photoreceptor signals are processed into virtual images, and the circadian system, in which light entrains a physiological clock. Here we describe a light response pathway in mice that employs encephalopsin (OPN3, a 480 nm, blue-light-responsive opsin) to regulate the function of adipocytes. Germline null and adipocyte-specific conditional null mice show a light- and *Opn3*-dependent deficit in thermogenesis and become hypothermic upon cold exposure. We show that stimulating mouse adipocytes with blue light enhances the lipolysis response and, in particular, phosphorylation of hormone-sensitive lipase. This response is *Opn3* dependent. These data establish a key mechanism in which light-dependent, local regulation of the lipolysis response in white adipocytes regulates energy metabolism.

INTRODUCTION

The detection of photons by animals has been exploited for adaptive advantage in many ways. The visual sense—irradiance detection by photoreceptors in the retina and formation of virtual images in the brain—is the most obvious example, because it is a component of our conscious existence. However, functioning in parallel in many types of animals are various non-visual ocular photoreceptors. In mammals, the best characterized are the retinal ganglion cells expressing melanopsin (Opsin 4 [OPN4]) and neuropsin (OPN5) that function in negative phototaxis (Johnson et al., 2010), circadian clock entrainment (Panda et al., 2002; Buhr et al., 2015), the pupillary light reflex (Hattar et al., 2002), and eye development (Nguyen et al., 2019; Rao et al., 2013).

Photoreceptors that function outside the eye are found throughout the animal kingdom. They exist as chromatophores in the skin of frogs (Moriya et al., 1996; Provencio et al., 1998), within the pineal organs that produce melatonin (Okano et al., 1994), and as deep brain photoreceptors that regulate seasonal breeding responses in avian species (Nakane et al., 2010). Extraocular photoreceptors were assumed to be absent from mammals until expression domains outside the eye were defined for OPN3, OPN4, and OPN5. Coupled with studies demonstrating light-dependent signaling (Kato et al., 2016; Kojima et al., 2011; Koyanagi et al., 2013; Yamashita et al., 2010) mammalian extraocular photoreception was proposed. We now know that OPN5 photoentrains the circadian clock in skin (Buhr et al., 2019) and that OPN4 can acutely regulate blood vessel dilation (Sikka et al., 2014, 2016). It has also been suggested that adipocyte function might be modulated by light stimulation of OPN4 (Ondrusova et al., 2017). Although attempts to express mammalian OPN3 have proven difficult, studies on its vertebrate ortholog from

pufferfish suggest that it may function as a photosensitive opsin (Koyanagi et al., 2013). Accumulating evidence points to extraocular photoreception via OPN3 in both mouse and human (Barreto Ortiz et al., 2018; Buscone et al., 2017; Castellano-Pellicena et al., 2019; Regazzetti et al., 2018; Yoshimoto et al., 2018).

Mammals employ three types of adipocytes (Giralt and Villarroya, 2013). White adipose tissue (WAT) consists primarily of white adipocytes and is the major energy storage site. Brown adipose tissue (BAT) is made up exclusively of brown adipocytes, which generate heat via non-shivering thermogenesis (NST) (Giralt and Villarroya, 2013). Under conditions of cold exposure, WAT can differentiate into "brite" adipocytes that have functional UCP1, although its capacity is at most a third of that of BAT (Rosenwald et al., 2013; Shabalina et al., 2013; Wu et al., 2012). The process of lipolysis releases free fatty acids (FFAs) and glycerol from WAT for systemic use (Zechner et al., 2012). BAT then uses FFAs for the generation of heat by oxidative uncoupling via UCP1 (Ikeda et al., 2017; Kazak et al., 2015, 2017a). Thus, WAT and BAT both have important functions in the regulation of energy balance. Though it was originally believed that only newborn humans had significant depots of brown fat, it is now understood to be present in the adult (Cypess et al., 2009; van Marken Lichtenbelt et al., 2009; Nedergaard et al., 2007; Virtanen et al., 2009). Gathering evidence suggests that activation of BAT might be valuable in protecting against metabolic syndrome (Harms and Seale, 2013; Seale, 2013).

Here we describe an extraocular function for OPN3 in the light-dependent regulation of adipocyte function. When cold challenged, mice with an adipocyte-specific deletion of *Opn3* fail to defend their body temperature normally, show an attenuated induction of cold-induced genes in BAT, and use less fat mass when fasted. Many of these phenotypes are reproduced in mice that are raised without the blue light wavelengths that normally stimulate OPN3. Furthermore, we show that blue light has an adipocyte-specific, acute stimulatory effect on thermogenesis. These metabolic perturbations appear to be explained by the OPN3 and blue light dependence of the lipolysis response, a pathway that normally provides fatty acid fuel for thermogenesis. These data identify an unanticipated mechanism for light information decoding for energy homeostasis.

RESULTS

OPN3 Is Expressed in Adipocytes

No reliable antibodies for murine OPN3 are presently available, so to assess expression of *Opn3*, we took advantage of three alleles (Figure S1): $Opn3^{lacz}$, $Opn3^{cre}$ (in combination with the tdTomato reporter *Ai14*), and *Opn3-eGFP*, an expression reporter transgene based on a bacterial artificial chromosome (GENSAT 030727-UCD). The interscapular adipose tissue (iAT) depot comprises interscapular subcutaneous white adipose tissue (iscWAT) and interscapular brown adipose tissue (iBAT). X-gal labeling of control cryosections from postnatal day (P) 16 iAT showed no background labeling in wild-type mice (Figure 1A) but intense labeling in the $Opn3^{lacz/lacz}$ iscWAT (Figure 1B). Labeled adipocytes were not detected in control iBAT (Figure 1C). In iBAT from $Opn3^{lacz/lacz}$, X-gal-labeled cells were not readily apparent, but at higher magnification and bright transillumination, a subset expressing brown adipocytes was detected (Figure 1D).

Neonatal inguinal white adipose tissue (inWAT) has a high content of brite adipocytes (Figures 1E and 1F, BrAd). In control P16 inWAT, neither the large unilocular white adipocytes nor the smaller brite adipocytes were X-gal labeled (Figures 1E and 1G). By contrast, the large, unilocular white adipocytes from $Opn3^{lacz/lacz}$ mice were X-gal positive (Figures 1F and 1H). When we used the $Opn3^{cre}$ allele (Figure S1) to convert the tdTomato reporter *Ai14* (Figures 1I–1K), cryosections showed that almost all adipocytes within iscWAT were positive (Figures 1I and 1K). In iBAT, a subset of brown adipocytes was positive (Figures 1J and 1K). The *Opn3-eGFP* reporter confirmed expression of *Opn3* in most white and brown adipocytes (Figure S2). Finally, Genotype-Tissue Expression (GTEx; accession phs000424.v7.p2, accessed on 02/21/2018) data report low to moderate expression of OPN3 in human subcutaneous and omental adipose tissue (2.9 and 3.1 tags/million, respectively) (Figure S2). These data indicate that both mouse and human adipose tissues express *Opn3* and raise the possibility of direct light responsiveness.

Photon Flux within iscWAT and iBAT Is Sufficient for Opsin Activation

To measure photon flux within the iAT of a pigmented mouse (Figure 2A), we fabricated the Holt-Sweeney microprobe (HSM) (Figure 2B) from a light-shielded optic fiber and attached a transparent spherical collecting tip, permitting omnidirectional measurements of scalar irradiance under constant angular sensitivity (Holt et al., 2014). The microprobe is mounted within a pulled Pasteur pipette and lowered into the iAT with a stereotaxic frame. Photon flux measurements across the 350–800 nm spectral range were taken every 0.5 mm up to a 2.5 mm total depth (Figure 2C). At the λ_{max} of 480 nm for OPN3 (Figure 2D), the measured photon flux was 5×10^{14} photons $cm^{-2}s^{-1}$ at 0.5 mm (deepest point within iscWAT) (Figure 2C) and 2×10^{13} photons $cm^{-2}s^{-1}$ at 2.5 mm (deepest point within iBAT) (Figure 2C). Surface illumination was controlled to 1% of clear sky sunlight intensity (direct sunlight intensity was measured to be 2×10^{17} photons $cm^{-2}s^{-1}$). Total light attenuation ranged from less than one log quanta at 0.5 mm to just over two log quanta at 2.5 mm. Extrapolating for full sunlight, iscWAT photon flux would be approximately 5×10^{16} photons $cm^{-2}s^{-1}$. Signaling thresholds for atypical opsins are as low as 10^{10} photons $cm^{-2}s^{-1}$ (Wong, 2012). Thus, these data indicate that iscWAT and iBAT photon flux is sufficient for opsin stimulation.

Transcriptome Analysis Suggests that *OPN3* Regulates Metabolism

To address OPN3 function, we performed a microarray-based transcriptome analysis on P16 control and *Opn3* germline null mice. iAT and inWAT were harvested alongside liver (low-expression control). Using the AltAnalyze suite (Emig et al., 2010; Salomonis, 2012), we identified *Z* score significant clustering of differentially regulated transcripts (red, upregulated; blue, downregulated) into select WikiPathway models (Figures S3A–S3C), with a more detailed schematic included (Figures S3D–S3H). As expected, the *Opn3* transcript showed the highest negative fold change in *Opn3* null iAT (3.0-fold down,

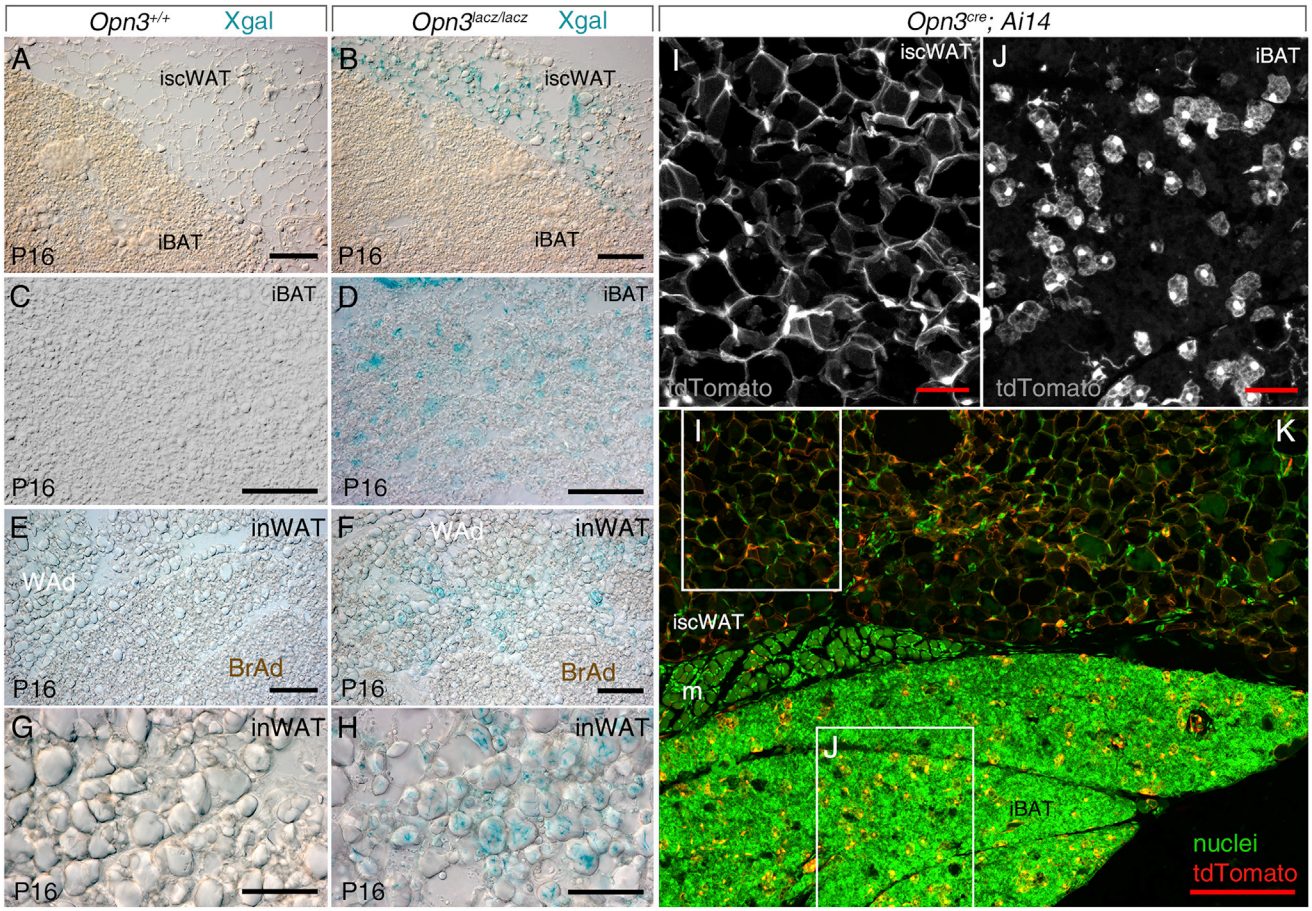

Figure 1. Expression of *Opn3* in iAT and inWAT

(A–D) X-gal-labeled wild-type (A and C) and *Opn3*$^{lacz/lacz}$ (B and D) cryosections of iAT, including iscWAT (A and B) and iBAT (C and D) at P16.

(E–H) X-gal-labeled wild-type (E and G) and *Opn3*$^{lacz/lacz}$ (F and H) cryosections of inWAT, including white adipocytes (WAd) and brite adipocytes (BrAd). (G and H) Higher magnification of inWAT in wild-type (G) and *Opn3*$^{lacz/lacz}$ (H) cryosections.

(I–K) Detection of tdTomato (red, grayscale) in *Opn3*^{cre}*; Ai14* mice for iAT showing positive cells in iscWAT (I, enlarged region in K) and iBAT (J, enlarged region in K). iscWAT and iBAT are separated by a leaflet of muscle (m). Labeling of nuclei with Hoechst 33258 is presented in green.

Scale bars: (A, B, E, F, and K) 100 μm and (C, D, and G–J) 50 μm.

$p = 1.5 \times 10^{-4}$) and inWAT (5.6-fold down, $p = 7.6 \times 10^{-3}$) but was not significantly changed in liver. Overall, transcriptome analysis indicated that OPN3 activity was required for normal regulation of metabolism, as evidenced by deregulation of the adipocyte extracellular matrix, lipid, glucose, and energy generation pathways.

In inWAT, *Opn3*-dependent, differentially regulated transcripts cluster within the peroxisome proliferator-activated receptor (PPAR) pathway and the mitochondrial electron transport chain (ETC) (Figure 3A). The PPAR pathway regulates adipocyte size, as well as lipid metabolism and energy generation (Fan and Evans, 2015; Liu et al., 2007). This pathway regulates energy generation in part because multiple components of the lipolysis pathway, including HSL (hormone-sensitive lipase), ATGL (adipose triglyceride lipase) (Leone et al., 1999; Rhee et al., 2003; Vega et al., 2000), and perilipin (PLIN) (Arimura et al., 2004), directly or indirectly depend on the transcriptional co-activator PGC1a for their expression. Furthermore, UCP1 is downregulated, presumably as a response to deregulation of its transcription factors PGC1a and RXRa/b (Puigserver et al., 1998). Notably, the transcript for lipoprotein lipase (*Lpl*), an enzyme with a role in extracellular lipolysis (Olivecrona, 2016) is deregulated in the liver of *Opn3* null mice (Figure S3). Finally, inWAT from *Opn3* null mice showed a striking cluster of 17 downregulated ETC transcripts (Figure 3A). Combined, these data suggest deregulated energy metabolism in *Opn3* null mice.

Detection of UCP1 in inWAT either by immunofluorescence (Figure 3B) or by immunoblot (Figure 3C) confirmed the comparatively low levels in *Opn3* null mice. inWAT cell-size assessment showed that *Opn3* null mice had, on average, larger adipocytes (Figure 3D). Hematoxylin inWAT staining also show lower proportions of the smaller brite adipocytes (Figure 3E), consistent with adipocyte size assessment.

We then measured total NAD content in *Opn3* null mice to assess mitochondrial function (Peek et al., 2013). Quantification showed no change in liver NAD in *Opn3* null mice but a reduction

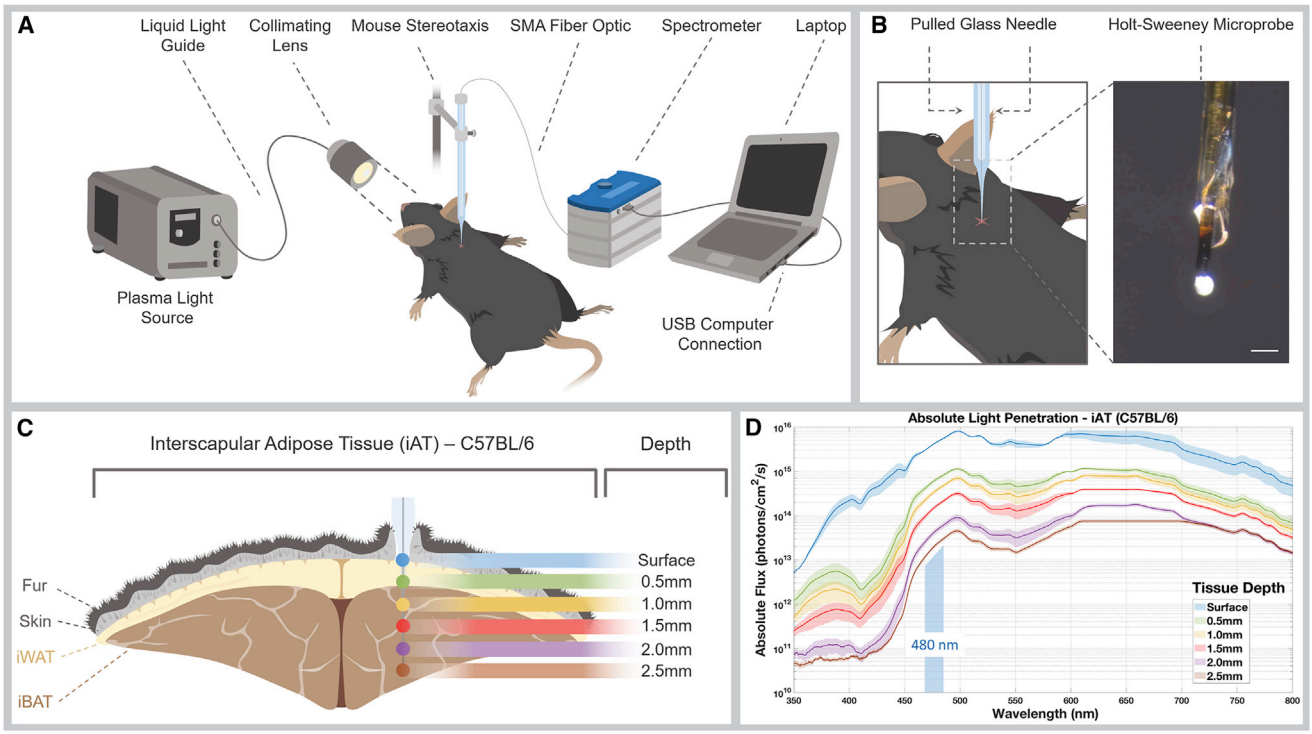

Figure 2. Measurement of Photon Flux within iBAT and iscWAT

(A) Schematic describing set up for measuring intra-tissue photon flux. Collimated photons from a plasma source are directed toward an anesthetized mouse, into which the fiber probe is guided via a stereotaxic frame. Spectra are measured by an OceanOptics spectrometer.

(B) Holt-Sweeney microprobe (scale bar: 100 μm) is an optic fiber with a transparent spherical tip that accepts photons over approximately 4π steradians.

(C) Measurement depths along iAT.

(D) Absolute photon flux within interscapular adipose color coded for depth. The uppermost blue trace is surface flux and, at the λ_{max} for OPN3, is about 2×10^{15} photons $cm^{-2}s^{-1}$. At the maximum 2.5 mm depth (brown trace), the flux at the OPN3 λmax is approximately 1×10^{13} photons $cm^{-2}s^{-1}$. Each trace is averaged data from n = 3 mice. Color shading is ±SEM.

in inWAT (Figure 3F), consistent with reduced mitochondrial content. Though transcriptome analysis for *Opn3* null iBAT did not cluster the ETC, we were prompted by the effects of *Opn3* deficiency on inWAT to assess mitochondrial status in iBAT. Immunoblotting for the ETC components ATP5A (Complex V), COX1 (Complex IV), SDHB (Complex II), NDUFB8 (Complex I), and UCP1 revealed some variability in the presence of SDHB in *Opn3* null mice but a consistently low level of both NDUFB8 and UCP1 (Figure 3G). Correspondingly, iBAT transmission electron microscopy (TEM) at P28 shows disorganized organellar cristae (Figure 3H), similar to that of *Ucp1* null mice (Kazak et al., 2017b), implying in part, *Opn3*-dependent changes in mitochondrial maintenance and/or organization.

To assess OPN3 function as a photoreceptive opsin, we raised C57BL/6J mice in "minus blue" lighting conditions from embryonic day (E) 16.5 (see STAR Methods) and compared them with mice raised under full spectrum conditions. Subtracting 480 nm wavelengths reduces total photon flux, but because opsins are sensitive to specific wavelengths, this lighting paradigm ensures that any non-blue opsin receives unchanged stimulation. Minus blue lighting resulted in inWAT with quantifiably larger adipocytes (Figure 3I), lower brite adipocyte content (Figure 3J), and lower total NAD (Figure 3K). Furthermore, minus blue iBAT showed lower levels of NDUFB8 and UCP1 (Figure 3L). When compared with *Opn3* null mice, the minus blue phenotype is milder. This might be explained by residual activation of OPN3 resulting from low-efficiency absorption of violet and red photons. Altogether, these data support the hypothesis that OPN3 functions as a light sensor that regulates adipose tissue development.

Adaptive Thermogenesis in Mice Is Promoted by Blue Light in an OPN3-Dependent Manner

In mice, body temperature is partly maintained by heat that is generated by skeletal muscle shivering or within BAT via NST pathways that employ UCP1, creatine metabolism, and calcium cycling (Ikeda et al., 2017; Kazak et al., 2015, 2017a). The energy for thermogenesis is provided partly by the oxidative metabolism of FFAs that are stored in adipocytes. The process of lipolysis liberating FFAs is thus crucial for normal NST (Himms-Hagen, 1972). Furthermore, it has been shown that lipolysis in white adipocytes is directly required to fuel NST (Schreiber et al., 2017; Shin et al., 2017). Several features of our *Opn3* null and minus blue mice suggested defects with NST.

When $Opn3^{+/+}$ and $Opn3^{lacz/lacz}$ neonatal mice were exposed to 4°C over the course of 3 h under full spectrum lighting, core body temperatures (CBTs) of *Opn3* null mice were lower than

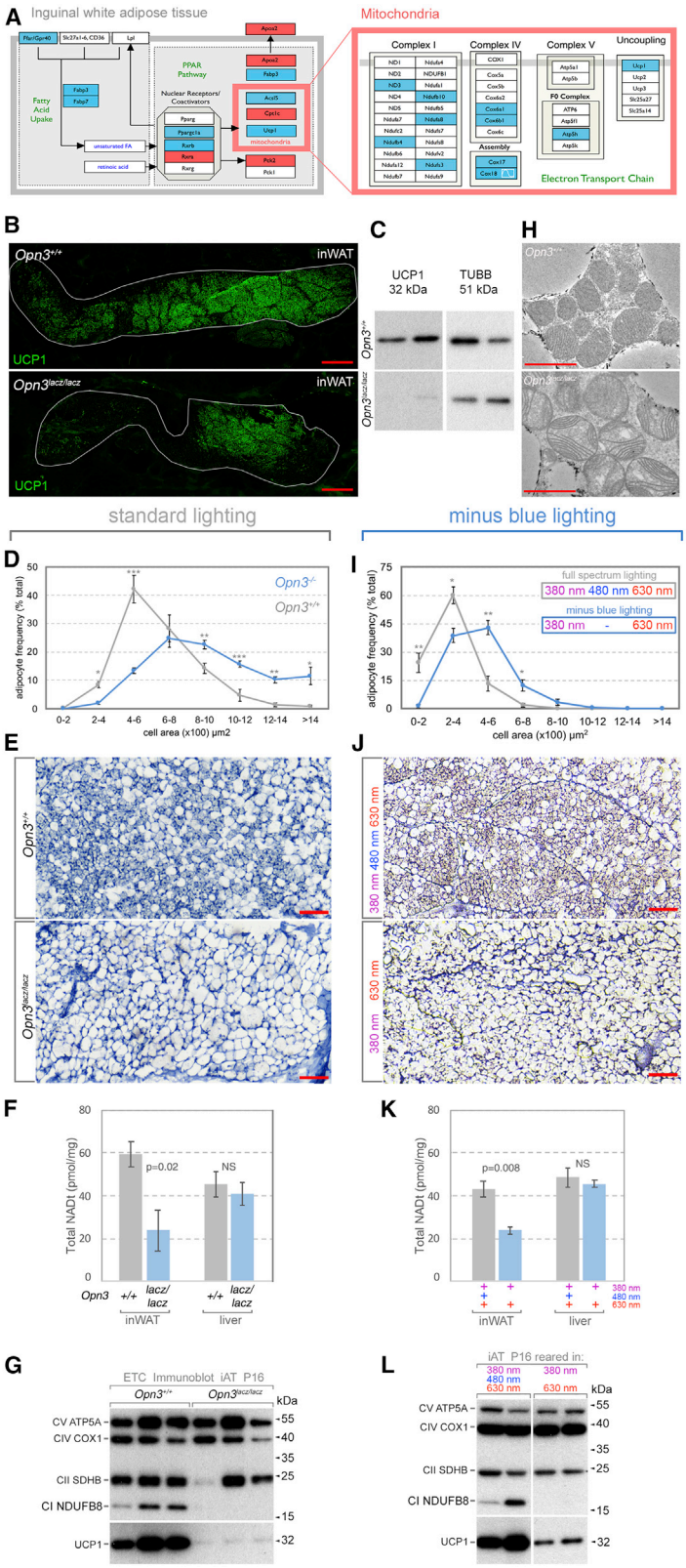

Figure 3. *Opn3* Null and Minus Blue Reared Mouse inWAT Phenotype

(A) Schematic of clustered *Opn3*-dependent transcript changes in PPAR (WP2316), lipid uptake, and mitochondrial ETC (WP295) pathways (red, upregulated; blue, downregulated).

(B) UCP1 (green) labeling of inWAT in control and $Opn3^{lacz/lacz}$ animals at P16.

(C) Immunoblot detecting UCP1 and β-tubulin (TUBB) in P16 inWAT from $Opn3^{+/+}$ and $Opn3^{lacz/lacz}$ mice.

(D–L) Adipocyte size distribution (D and I) in inWAT comparing control and $Opn3^{lacz/lacz}$ (D) and full spectrum versus minus blue raised (I) mice at P16. Data are presented as mean ± SEM, n = 3 for each genotype. Direct comparisons between genotypes at each interval were performed with Student's t test, *p < 0.05, **p < 0.01, ***p < 0.001.

(E and J) Hematoxylin staining of histological sections of P16 inWAT from $Opn3^{+/+}$, $Opn3^{lacz/lacz}$ (E) and full spectrum (380, 480, and 630 nm) reared versus minus blue (380 and 630 nm) reared (J) mice.

(F and K) Total NAD levels in inWAT and liver for P16 $Opn3^{+/+}$ and $Opn3^{lacz/lacz}$ mice (F, n = 4) or for mice reared either in full spectrum or minus blue lighting (K, n = 3). p values calculated using Student's t test.

(G and L) Immunoblots detecting multiple components of the ETC (ATP5A, COX1, SDHB, NDUFB8, and UCP1) in P16 iAT for $Opn3^{+/+}$, $Opn3^{lacz/lacz}$, and minus blue reared mice.

(H) TEM showing abnormal mitochondrial morphology in the *Opn3* null iBAT at P28.

Scale bars: (B) 500 µm, (E and J) 100 µm, and (H) 2 µm.

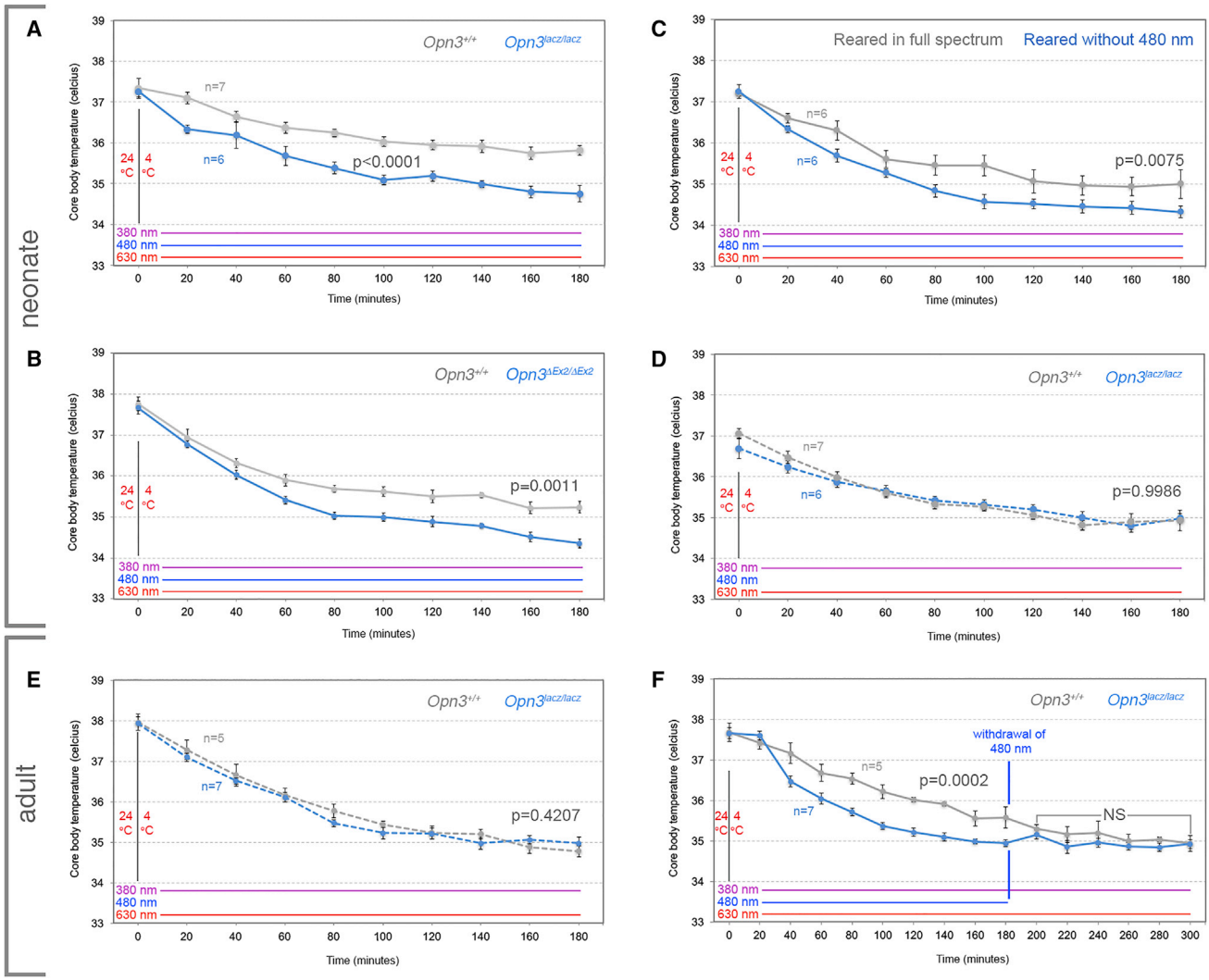

Figure 4. *Opn3* Is Required for Light-Dependent Enhancement of the Thermogenesis Response

CBT assessments over a time course after a 4°C cold exposure for P21–P24 (neonatal) or adult mice of the indicated genotypes. Lighting conditions during cold exposure are indicated by the colored lines above the chart's horizontal axis.

(A) CBTs during cold exposure in *Opn3*$^{lacz/lacz}$ and control *Opn3*$^{+/+}$ in full spectrum (380 + 480 + 630 nm) lighting.

(B) CBTs during cold exposure in *Opn3*$^{\Delta Ex2/\Delta Ex2}$ and control *Opn3*$^{+/+}$ C57BL/6J background mice in full spectrum lighting.

(C) CBTs during cold exposure for C57BL/6J mice raised either in full spectrum (gray trace) or in minus blue (380 + 630 nm, blue trace) lighting.

(D) CBTs during cold exposure in the same cohorts of mice shown in (A) except in minus blue lighting.

(E) As in (D) except for adult mice (2 months).

(F) CBTs during cold exposure in *Opn3*$^{lacz/lacz}$ and control *Opn3*$^{+/+}$ in full spectrum (380 + 480 + 630 nm) lighting for 180 min and minus blue (480 nm withdrawn) lighting for a further 120 min.

Data are presented as mean ± SEM.

those of wild-type mice (Figure 4A). To account for possible thermogenic influences caused by the mixed genetic background of *Opn3*$^{lacz/lacz}$ mice, we generated a new *Opn3* loss-of-function allele on a pure C57BL/6J background by CRISPR (*Opn3*$^{\Delta Ex2}$) and repeated the analysis. *Opn3*$^{\Delta Ex2/\Delta Ex2}$ mice also show lower defended CBTs (Figure 4B), confirming the reduction in NST to be *Opn3* dependent. We could again test the assertion that OPN3 functions as a light sensor by assessing NST in minus blue mice. After 3 h of cold exposure, minus blue mice similarly showed lower defended CBTs than mice reared under full spectrum lighting (Figure 4C). These data show that the absence of 480 nm light that normally stimulates OPN3 during development mimics genetic loss of function.

At the same time, it was possible that OPN3 could mediate acute light responses. We tested this by cold exposing the same cohort of *Opn3* wild-type and null mice (Figure 4A) under minus blue lighting. Interestingly, the CBTs of control and *Opn3* null mice were statistically indistinguishable (Figure 4D). This suggested that blue light can, via OPN3, acutely promote adaptive NST and that the activity of OPN3 is necessary for this effect.

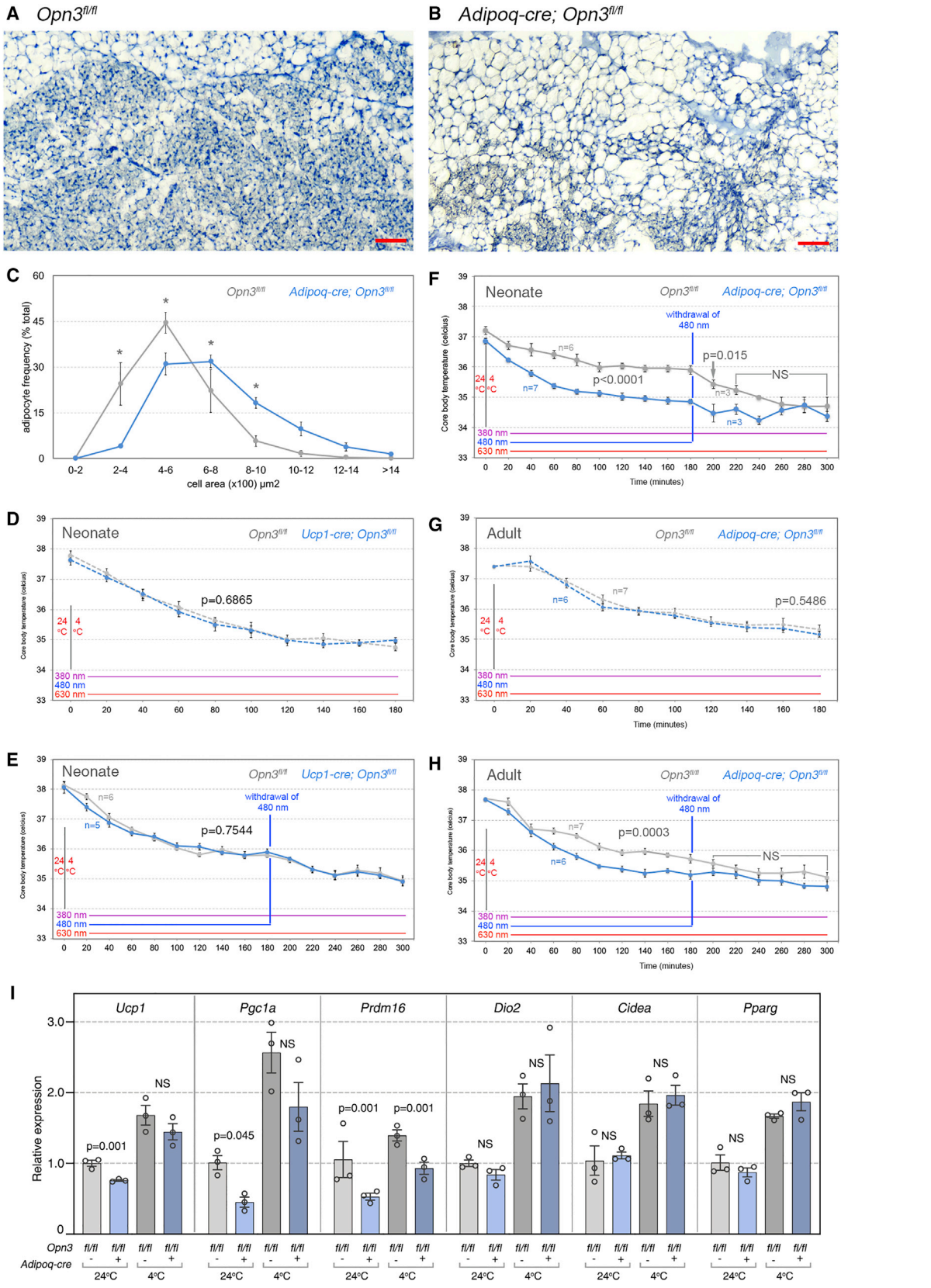

(legend on next page)

Neonatal mice have a beige adipocyte content that is higher than it is in adult mice (Sanchez-Gurmaches et al., 2012; Xue et al., 2007), and this may reflect special NST requirements given their low mass-to-surface area ratio. Thus, we also sought to establish whether adult mice showed a blue-light-promoted, OPN3-dependent NST response. For this analysis, we performed two types of experiments. In the first, we assessed CBTs in cohorts of adult control and *Opn3* null mice in the minus blue condition and showed that they were indistinguishable (Figure 4E). Then, with the same cohorts of mice, we repeated the assessment in full spectrum lighting and showed that over 3 h of cold exposure, wild-type mice CBTs were higher than those of *Opn3* null mice (Figure 4F, to minute 180). This shows that as in neonatal mice, adult NST is promoted by light and by OPN3 activity. At minute 180, we turned off the 480 nm light and observed a decrease in CBTs of wild-type mice to become indistinguishable from that of *Opn3* null mice. This provides further evidence that blue light can acutely regulate adaptive thermogenesis in an OPN3-dependent manner and that this can occur in both neonatal and adult mice.

White Adipocyte *Opn3* Is Required for a Normal Thermogenesis Response

To determine whether we could attribute aspects of the germline null phenotype to adipocyte *Opn3*, we conditionally deleted *Opn3* with pan-adipocyte *Adipoq-cre* (Eguchi et al., 2011). The inWAT of neonatal *Adipoq-cre; Opn3*$^{fl/fl}$ mice shows low beige content (Figures 5A and 5B) and larger adipocyte size distribution (Figure 5C) similar to *Opn3*$^{lacz/lacz}$ and minus blue mice. This is consistent with the hypothesis that OPN3 functions as a light sensor within adipocytes to regulate adipose tissue development.

Because both brown and white adipocytes express *Opn3*, it was possible that the reduced NST in *Opn3* null mice could be explained by either BAT or WAT defects (or both). Thus, we measured CBTs in cohorts of neonatal mice in which *Opn3* was conditionally deleted either from only brown adipocytes with *Ucp1-cre* (Kong et al., 2014) or from all adipocytes with *Adipoq-cre*. We first confirmed efficient cre-mediated deletion of the floxed region of *Opn3* in both *Ucp1-cre; Opn3*$^{fl/fl}$ and *Adipoq-cre; Opn3*$^{fl/fl}$ mice by PCR (Figure S5A). Cold-exposed *Ucp1-cre; Opn3*$^{fl/fl}$ mice had CBTs indistinguishable from those of control *Opn3*$^{fl/fl}$ mice in any lighting condition (Figures 5D and 5E). This indicated that brown adipocyte *Opn3* was not required for normal NST.

By contrast, neonatal *Adipoq-cre; Opn3*$^{fl/fl}$ mice in full spectrum lighting showed a more limited ability than *Opn3*$^{fl/fl}$ control mice to defend their body temperature (Figure 5F). When 480 nm light was withdrawn at minute 180, CBTs of *Opn3*$^{fl/fl}$ mice rapidly dropped to the level of the conditional null (Figure 5F). Repetition of cold exposure experiments in adult *Opn3*$^{fl/fl}$ and *Adipoq-cre; Opn3*$^{fl/fl}$ null mice showed a similar thermogenesis deficit (Figures 5G and 5H) in which the absence of blue light, either throughout the cold exposure (Figure 5G) or acutely at minute 180 (Figure 5H), could mimic the conditional loss of adipocyte *Opn3*. The absence of an NST deficit in *Rx-cre; Opn3*$^{fl/fl}$ mice (Figure S5B), in which *Opn3* is conditionally deleted from retinal neurons, confirms that retinal OPN3 is not necessary for this pathway. Furthermore, unchanged tail temperature measured via infrared thermography in *Adipoq-cre; Opn3*$^{fl/fl}$ mice (Figure S5C) indicates that the observed CBT differences are unlikely to be a consequence of cutaneous vasodilation and conductive heat loss. Finally, qPCR assessment of a set of thermogenesis pathway transcripts (*Ucp1*, *Pgc1a*, *Prdm16*, *Dio2*, *Cidea*, and *Pparg*) in iAT showed, consistent with transcriptome analysis and the NST deficit, that loss of adipocyte *Opn3* resulted in diminished expression of *Ucp1*, *Pgc1a*, and *Prdm16* (Figure 5I). Combined, these data suggest that *Opn3* expression in white adipocytes, but not in retina or BAT, is required for the light-dependent component of the thermogenesis response.

Loss of *Opn3* Results in Decreased Energy Expenditure

To determine how *Opn3* contributes to longitudinal energy balance and homeostasis, we performed indirect calorimetry in 4-month-old *Opn3*$^{+/+}$ (n = 5) and *Opn3*$^{lacz/lacz}$ (n = 10) male mice. Animals were acclimated and individually housed in metabolic chambers (TSE Systems, PhenoMaster Cages), to assess energy expenditure at 22°C, 16°C, 10°C, and 30°C (Figure 6A). On average, *Opn3*$^{lacz/lacz}$ mice showed lower oxygen consumption (Figure 6B) and carbon dioxide expiration (Figure 6C) than controls, with the differences becoming significant at the lowest ambient temperatures ($p = 0.03$ and $p = 0.04$ for O_2, separate repeated-measures ANOVA conducted across a 5-h period during lights off and lights on, respectively). These differences disappeared once the ambient temperature was restored to thermoneutrality (30°C), suggesting that these differences represent adaptive, not pathological, responses. Correspondingly, *Opn3*$^{lacz/lacz}$ animals show lower energy expenditure (Figure 6D), with significant differences at 10°C. Unnormalized energy expenditure data (Figures S4A–S4C) also argue for differences

Figure 5. White Adipocyte *Opn3* Is Required for a Normal Thermogenesis Response

(A and B) Hematoxylin staining of *Opn3*$^{fl/fl}$ (A) and *Adipoq-cre; Opn3*$^{fl/fl}$ (B) inWAT at P16.

(C) Adipocyte size assessment in *Opn3*$^{fl/fl}$ and *Adipoq-cre; Opn3*$^{fl/fl}$ inWAT at P16. * = $p < 0.05$ by Student's *t* test.

(D–H) CBT assessments over a time course after a 4°C cold exposure for adult mice of the indicated genotypes. Lighting conditions during cold exposure are indicated by the colored lines above the chart's horizontal axis.

(D and E) CBTs of *Opn3*$^{fl/fl}$ and *Ucp1-cre; Opn3*$^{fl/fl}$ mice (D) under minus blue conditions and (E) in full spectrum lighting for 180 min and then for a further 120 min in minus blue.

(F) As in (E) except for cohorts of neonatal *Adipoq-cre; Opn3*$^{fl/fl}$ and control *Opn3*$^{fl/fl}$ mice.

(G) As in (D) except for cohorts of adult *Adipoq-cre; Opn3*$^{fl/fl}$ and control *Opn3*$^{fl/fl}$ mice.

(H) As in (F) except for adult mice.

(I) Relative expression of transcripts for the thermogenesis pathway genes *Ucp1*, *Pgc1a*, *Prdm16*, *Dio2*, *Cidea*, and *Pparg* in iBAT from mice of the indicated genotypes. iBAT was harvested from control mice in ambient temperature (24°C) and those exposed to 4°C for 3 h.

Data are presented as mean ± SEM. Scale bars: 100 μm.

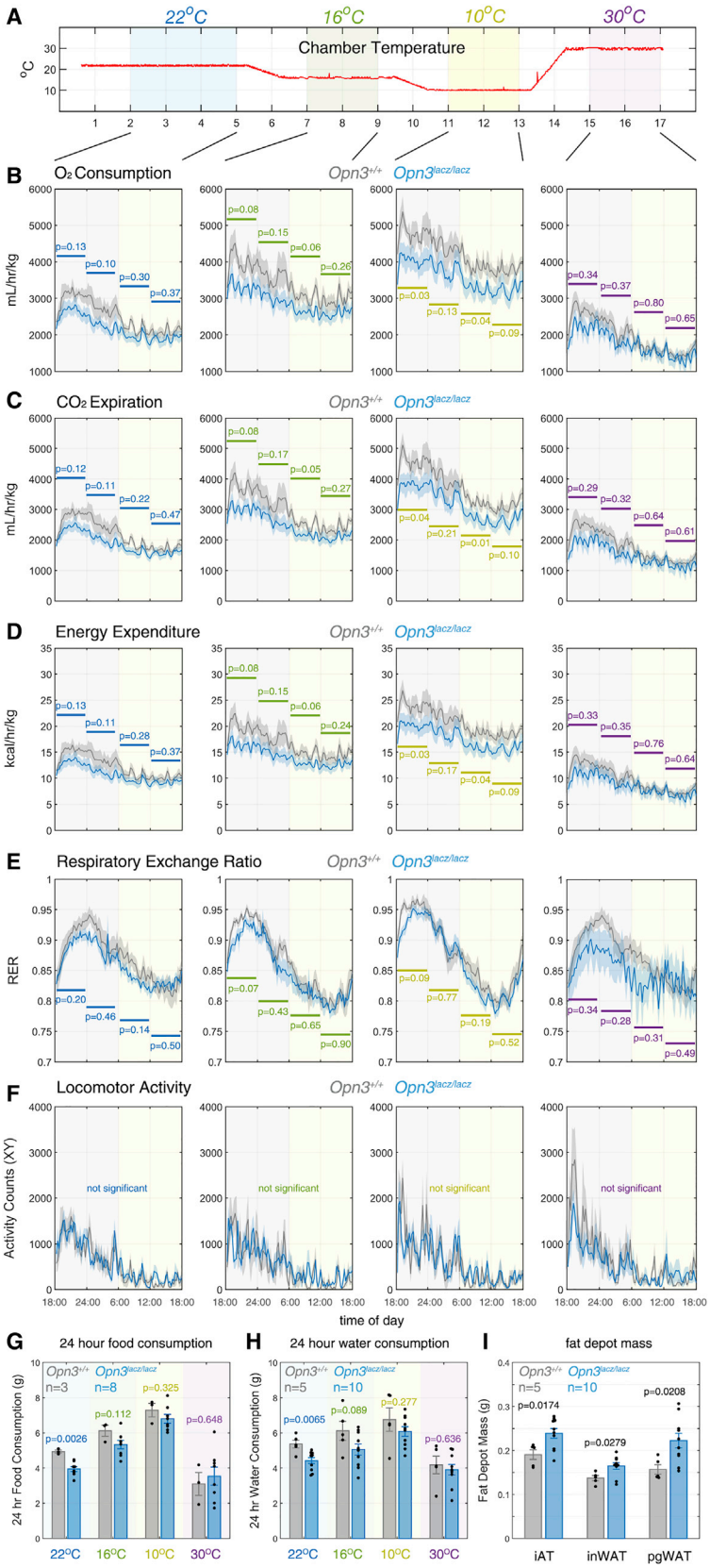

Figure 6. Loss of *Opn3* Alters Energy Metabolism

(A) Schematic detailing the ambient temperature throughout the experiment and the durations of measurement intervals.

(B–D) VO_2 (B), VCO_2 (C), and energy expenditure (EE, D) measurements by indirect calorimetry (TSE Systems, PhenoMaster Cages) were obtained for 22°C, 16°C, 10°C, and 30°C from *Opn3*$^{+/+}$ (gray trace, n = 5) and Opn3$^{lacz/lacz}$ (blue trace, n = 10) animals. Each graph shows a 24-h period of averaged data ± SEM for the corresponding ambient temperature. The lighting conditions were maintained at a standard 12L:12D cycle, depicted as lights off 6PM–6AM (gray shaded region) followed by lights on 6AM–6PM (yellow shaded region).

(E) Respiratory exchange ratio (RER) was calculated by the ratio VCO_2/VO_2.

(F) Spontaneous locomotor activity (XY) was measured by infrared beam breaks.

(G and H) 24-h average food (G) and water consumption (H) were measured by differential weight-based sensors and plotted per ambient temperature.

(I) Postmortem fat depot masses in iAT, inWAT, and pgWAT. All statistics performed on the data in (B)–(F) are repeated-measures ANOVA across 5-h time intervals: 7PM–12AM, 12AM–5AM, 7AM–12PM, and 12PM–5PM.

Statistics performed on the data in (G)–(I) are 2-way ANOVAs with p values reported from Holm-Šídák corrected multiple comparisons.

in energy expenditure between *Opn3*$^{+/+}$ and *Opn3*$^{lacz/lacz}$ mice that are exacerbated by decreasing ambient temperature.

The respiratory exchange ratio (RER) was estimated by calculating the ratio of VCO_2/VO_2 and was not significantly changed between *Opn3*$^{+/+}$ and *Opn3*$^{lacz/lacz}$ animals throughout the experiment. This suggests the absence of substrate utilization preference and reflects the overall decreased metabolic demand caused by the loss of *Opn3*. This is supported by the lack of locomotor activity differences between *Opn3*$^{+/+}$ and *Opn3*$^{lacz/lacz}$ animals (Figure 6F), which decouples the observed changes in energy expenditure from gross activity levels. In addition, locomotor activity data strongly suggest the absence of change in circadian phasing between *Opn3*$^{+/+}$ and *Opn3*$^{lacz/lacz}$ animals, implying that loss of *Opn3* does not result in an altered activity cycle. Finally, *Opn3*$^{lacz/lacz}$ animals consumed less food (Figure 6G) and water (Figure 6H) compared with controls, consistent with their lower energy expenditure. Postmortem fat depot masses were higher in the *Opn3*$^{lacz/lacz}$ animals, perhaps suggesting diminished fat mobilization (Figure 6I). Altogether, these data argue for the importance of OPN3 for adaptive thermogenesis, with direct consequences for whole-organism energy storage and utilization.

White Adipocyte OPN3 Is Required for Normal Lipolysis during Cold Exposure

The long-standing belief that BAT lipolysis is essential for NST has been challenged by recent analyses (Schreiber et al., 2017; Shin et al., 2017) showing that inhibiting lipolysis in BAT does not compromise defended CBTs as long as WAT or cardiac muscle lipolysis is intact. Because this distinction mimicked the CBT differences between our *Ucp1-cre; Opn3*$^{fl/fl}$ and *Adipoq-cre; Opn3*$^{fl/fl}$ mice, we asked whether *Opn3* in white adipocytes was necessary to provide thermogenic fuel during cold exposure. This was addressed with two complementary approaches: First, we performed an *in vivo* fasting experiment aimed at augmenting the use of fat reserves via lipolysis during cold exposure (Shin et al., 2017; Schreiber et al., 2017).

In this analysis, cohorts of control (*Opn3*$^{fl/fl}$) and experimental (*Adipoq-cre; Opn3*$^{fl/fl}$) mice were either fed *ad libitum* or fasted overnight and then exposed to 4°C for 3 h (Figure 7A). At the termination of the experiment, fat depots were dissected and weighed. After subtracting fat mass differences between fed and fasted animals, we found that *Adipoq-cre; Opn3*$^{fl/fl}$ animals mobilized significantly less fat mass than controls (380 versus 230 mg iAT, 380 versus 180 mg inWAT, and 300 versus 33 mg perigonadal white adipose tissue [pgWAT]) (Figure 7C). This was consistent with the hypothesis that adipocyte *Opn3* is required for a normal utilization of fat mass. Fat mass changes under conditions of fed versus fasting state have been documented previously (Syamsunarno et al., 2014) and illustrate the need for lipolysis under conditions of nutritional deprivation.

Lipolysis is initiated by β-adrenergic receptor activation of Gαs and adenyl cyclase (Carey, 1998). This elevates cyclic AMP (cAMP) and engages targets of protein kinase A (PKA), including HSL, PLIN, and cAMP response element-binding protein (CREB), liberating glycerol and FFAs from stored triglycerides (Rogne and Taskén, 2014). Fasted mice showed significantly elevated serum glycerol compared with fed mice, but this difference was diminished in *Adipoq-cre; Opn3*$^{fl/fl}$ mice compared with controls (Figure 7D). Assessment of cAMP from inWAT lysates revealed that control mice show significantly elevated cAMP compared with *Adipoq-cre; Opn3*$^{fl/fl}$ mice during the light phase of a 12:12 h light-dark (12L:12D) cycle (Figure 7E). However, this difference was abolished during the dark phase. Thus, both measurements of serum glycerol and cAMP in inWAT support the hypothesis that OPN3 is required for a light-dependent regulation of the lipolysis response.

In our second approach, we asked whether adipocytes could respond to light in isolation. Therefore, we differentiated adipocytes from the stromal vascular fraction (SVF) of inWAT from *Opn3*$^{+/+}$ and *Opn3*$^{lacz/lacz}$ mice. cAMP measurements from these white adipocytes follow a dose-dependent response to photon flux (Figure 7F). We then exposed cultured adipocytes of both genotypes to 480 nm light and compared levels of phosphorylated PKA substrates to unexposed cultures. We observed consistently elevated phosphorylated HSL (phospho-HSL) in light-stimulated *Opn3*$^{+/+}$ adipocytes compared with dark ones (Figure 7G). However, this light-dependent elevation was absent from *Opn3*$^{lacz/lacz}$ adipocytes. Quantification of this response shows significantly higher light-induced phospho-HSL in *Opn3*$^{+/+}$, but not *Opn3*$^{lacz/lacz}$, cultured adipocytes (Figure 7H). Light-induced *Opn3*-dependent changes in other PKA targets were also observed (Figure S5D). We also measured free glycerol in culture media from differentiated white adipocytes and found a significant elevation of free glycerol in blue-light-stimulated control adipocytes (Figure 7I), but not *Opn3* null adipocytes (Figure 7J). These data argue for direct light responsiveness in isolated adipocytes that requires OPN3.

It has previously been suggested that OPN4 can mediate light responses in cultured primary adipocytes (Ondrusova et al., 2017). We therefore explored the possibility of OPN3-OPN4 interaction in light-mediated adipocyte function. Assessment of *Opn4* expression in iscWAT and iBAT from *Opn4*^{cre}*; Z/EG* (Ecker et al., 2010) mice revealed no lineage marking in adipocytes (Figures S5F and S5G), despite a robust signal in the retina (Figure S5E). To address a potential role for OPN4 in NST, we measured CBTs in cold-exposed cohorts of *Opn4* wild-type and null mice but found no significant differences (Figure S5H). Finally, we stimulated differentiated adipocytes from *Opn4*$^{+/+}$ and *Opn4* null inWAT with blue light and showed a robust induction of phospho-HSL in both (Figure S5I). These data were inconsistent with an *in vivo* role for adipocyte OPN4 in local light responses. We also tested the involvement of Rhodopsin (Opsin 2 [OPN2]), the photopigment-mediating vision under dim light, in defending CBTs on cold exposure. We used a mouse with a P23H mutation in the *Opn2* gene that produces a nonfunctional Rhodopsin protein (Sakami et al., 2011) (Figures S5J and S5K). Assessment of defended CBTs during cold exposure revealed no significant differences (Figure S5L). These data argue against a nonvisual function of OPN2 in NST.

DISCUSSION

We present an assessment of OPN3 (Blackshaw and Snyder, 1999; Koyanagi et al., 2013) (encephalopsin) function in the

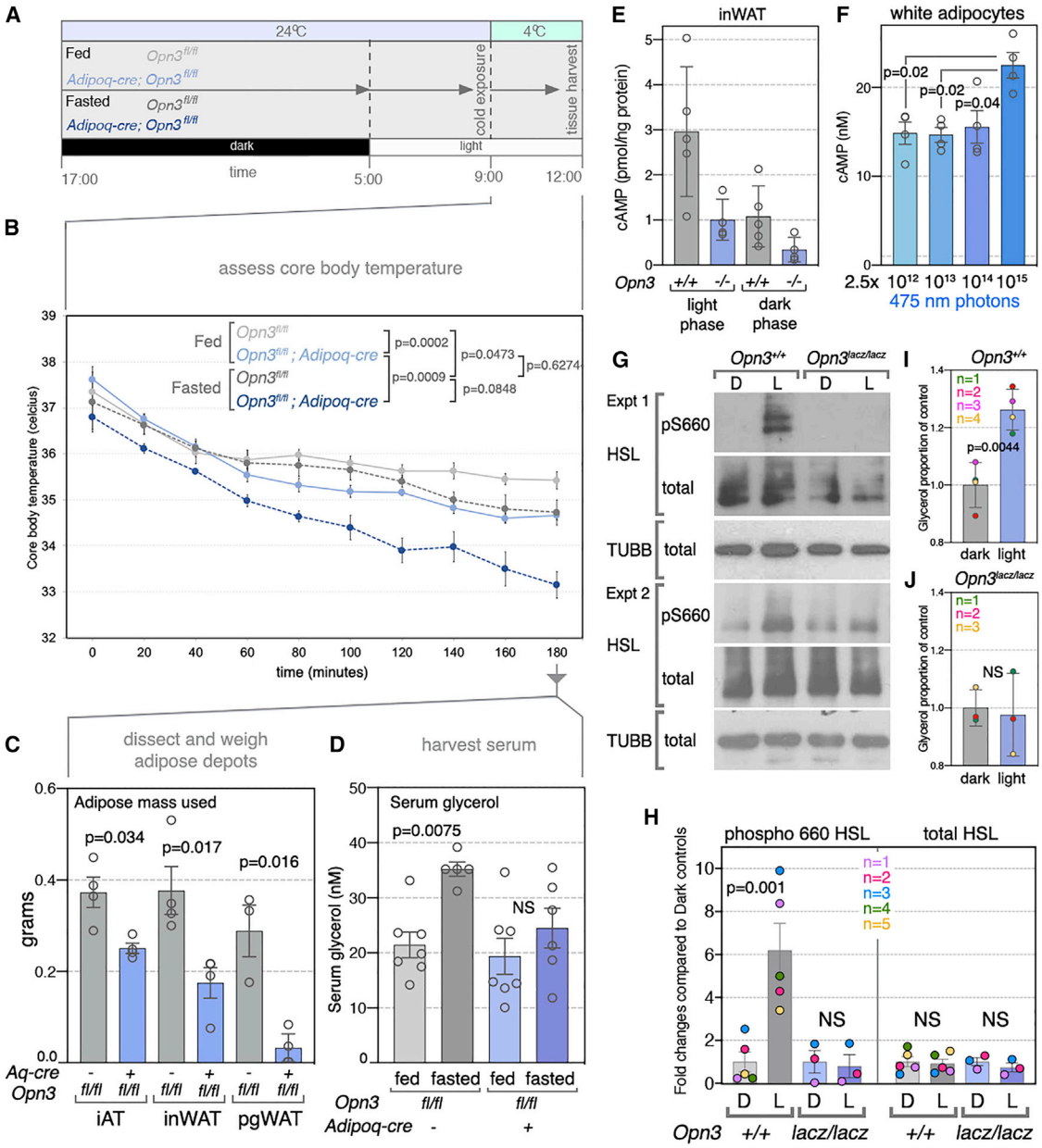

Figure 7. *Opn3*-Dependent Fat Mass Utilization *In Vivo* and Light- and *Opn3*-Dependent Lipolysis Activation *In Vivo* and *In Vitro*

(A) Schematic describing the timeline of a fasting-cold exposure experiment.

(B) CBT of fed and fasted *Opn3*$^{fl/fl}$ and *Adipoq-cre; Opn3*$^{fl/fl}$ mice during 180 min of cold exposure.

(C) Fat mass used by *Opn3*$^{fl/fl}$ and *Adipoq-cre; Opn3*$^{fl/fl}$, fed and fasted, cold-exposed mice.

(D) Serum glycerol levels from the same fed and fasted *Opn3*$^{fl/fl}$ and *Adipoq-cre; Opn3*$^{fl/fl}$ mice as in (C) after the 180 min of cold exposure.

(E) Chart showing that *Opn3*$^{+/+}$ mice have elevated cAMP levels in lysates of inWAT during the light phase versus the dark phase, while the cAMP levels in the inWAT of *Opn3*$^{lacz/lacz}$ mice are similar in both phases, comparable to levels observed in the *Opn3*$^{+/+}$ dark phase and significantly lower than those seen in the *Opn3*$^{+/+}$ light phase.

(F) Cultured *in vitro* differentiated adipocytes show 475 nm light-dependent, dose-response elevation of cAMP.

(G) Two examples of immunoblots showing light-dependent and *Opn3*-dependent induction of phospho-660-HSL in cultured *in vitro* differentiated adipocytes. Each set of immunoblots (experiment 1 and experiment 2) was performed using white adipocytes isolated from separate mice.

(H) Quantification of phospho-HSL induction in wild-type control (*Opn3*$^{+/+}$, n = 5 mice) and *Opn3* loss-of-function (*Opn3*$^{lacz/lacz}$, n = 3 mice) white adipocytes.

(I and J) Quantification of glycerol released from *in vitro* differentiated *Opn3*$^{+/+}$ (I) and *Opn3*$^{lacz/lacz}$ (J) cells in response to 2 h of blue light stimulation compared with darkness.

mouse, in which adipocytes use OPN3-dependent light sensing to regulate metabolic physiology. Extraocular photoreception has been described in many species, including vertebrates such as fish (Kojima and Fukada, 1999; Sato et al., 2016) and birds (Nakane et al., 2010). To date, however, there are only a few documented examples of extraocular light reception in mammals. It has been argued that non-canonical opsins function within adipocytes (Ondrusova et al., 2017) and within the skin (Buhr et al., 2019; Buscone et al., 2017; Castellano-Pellicena et al., 2019; Regazzetti et al., 2018) and that they can mediate a vasorelaxation response (Sikka et al., 2014, 2016) and induce autophagy in human colon cancer cells (Yoshimoto et al., 2018). In this report, our data argue that adipocyte OPN3 has an important role in regulating lipid homeostasis.

OPN3 Activity Mediates a Light-Dependent Pathway that Regulates Energy Metabolism

OPN3 has all the crucial molecular characteristics of the opsin family of light-responsive G protein-coupled receptors (Koyanagi et al., 2013). Thus, one hypothesis to explain the *Opn3* phenotype places OPN3 as the candidate detector for decoding light information to regulate energy homeostasis. We tested this by raising C57BL/6J mice in minus blue conditions that exclude 480 nm wavelengths known to stimulate OPN3 homologs in other vertebrates (Koyanagi et al., 2013). Remarkably, minus blue mice show the same abnormal WAT histology and low NAD, reduced iAT ETC complexes, low UCP1, and NST deficits characteristic of *Opn3* null mice. This outcome is consistent with the existence of an OPN3-dependent, light-decoding metabolic regulation pathway. It suggests that OPN3 functions during development to establish the histological and functional characteristics of metabolic tissues.

A characteristic of non-canonical opsins is that they can mediate acute responses to light. OPN4 mediates the pupillary light reflex (Hattar et al., 2002) and light-aversive behavior in neonatal mice (Johnson et al., 2010). We showed that OPN3 could mediate light responses over a similar timescale by demonstrating light- and OPN3-dependent changes in CBTs during cold exposure. When we withdrew blue light, we showed that wild-type mice rapidly reduced their CBTs to abnormally low *Opn3* null levels. In this assessment, CBTs of *Opn3* null and wild-type mice were indistinguishable in minus blue conditions, indicating that OPN3 activity is necessary for the acute enhancement of body temperature by blue light. However, because minus blue reared animals also show deficits in NST, even under blue light stimulation (Figure 4C), OPN3 likely possesses additional developmental roles that are not addressed in the current study.

Acute light stimulation enhances body temperature in humans (Cajochen et al., 2000; Dijk et al., 1991), and this response is mediated by 460 nm light, but not 550 nm light (Cajochen et al., 2005). Though OPN4 has been implicated due to known circadian regulation of CBTs, the current analysis suggests the alternative hypothesis that OPN3-dependent light responses are central to this physiology. Analysis in *Drosophila*, demonstrating that acute light exposure causes elevated temperature preference (Head et al., 2015), suggests that this configuration of light information decoding is deeply conserved. Humans differ from mice in that we are a diurnal species, and the metabolic interaction between OPN3 and human circadian clock remains an open question. Even so, it is very likely that the activity of OPN3 in the light-dependent regulation of metabolic pathways and body temperature will be tightly integrated with OPN4-dependent circadian and ocular photic input pathways that also regulate this physiology (Rupp et al., 2019).

White Adipocytes Are a Site of OPN3 Metabolic Activity

Many cell types express *Opn3* (Blackshaw and Snyder, 1999; Nissilä et al., 2012; Regard et al., 2008; Sikka et al., 2016), and this raises the possibility that extraocular light reception in mammals is commonplace. In the current study, we have shown that white adipocytes are a crucial site of OPN3 function for NST. Although we excluded brown adipocyte *Opn3* activity from involvement in NST, there are likely to be adipocyte-independent activities of OPN3 not identified by the current analysis.

Prompted partly by transcriptome analysis, we showed that lipolysis in cultured white adipocytes is enhanced by blue light in an OPN3-dependent manner. As illustrated by the lower-than-normal body temperature that results when lipid mobilization enzymes are compromised (Schreiber et al., 2017), lipolysis is an essential component of a normal thermogenesis response in mice. Blue-light-stimulated white adipocytes show elevated cAMP and, importantly, dramatic elevation of phospho-HSL, the rate-limiting enzyme in the lipolysis pathway (Langin et al., 1996), a response lost in *Opn3* null adipocytes. Because lipolysis is an essential response for normal body temperature maintenance (Shin et al., 2017, 2018) and the resulting FFAs are required for the activation of UCP1 (Cannon and Nedergaard, 2004; Divakaruni and Brand, 2011; Fedorenko et al., 2012; Gonzalez-Hurtado et al., 2018), these findings provide, at least partly, a mechanistic explanation for the OPN3-dependent deficit in NST. Although we still do not fully understand the biochemistry of OPN3 receptor coupling and signaling in adipose tissue, the reduced ability of *Adipoq-cre; Opn3*$^{fl/fl}$ mice to use fat mass in response to fasting and cold exposure is consistent with a role for OPN3 in enhancing lipolysis *in vivo*. It would thus be crucial for future work to elucidate the specific OPN3-dependent signaling mechanisms in adipose tissue, enabling a better understanding of the direct link between blue-light-sensing OPN3 and lipolytic enzymes.

There is a growing body of evidence that OPN3 mediates light-dependent regulation of cellular physiology in mice and diverse human cell types (Barreto Ortiz et al., 2018; Buscone et al., 2017; Regazzetti et al., 2018; Yoshimoto et al., 2018). We now provide key evidence that OPN3 can regulate physiology at the organismal level, at least in the mouse. Both the primary amino acid sequence and the expression pattern of OPN3 are highly conserved. If the light-OPN3 adipocyte pathway exists in humans, there are potentially broad implications for human health. Our modern lifestyle subjects us to unnatural lighting spectra, exposure to light at night, shift work, and jet lag, all of which result in metabolic disruption (Fonken and Nelson, 2014; Fonken et al., 2013; Laermans and Depoortere, 2016; Opperhuizen et al., 2017). Based on the current findings, it is possible that insufficient stimulation of the light-OPN3 adipocyte pathway is part of an explanation for the prevalence of metabolic deregulation in industrialized nations where unnatural lighting has become the norm.

STAR★METHODS

Detailed methods are provided in the online version of this paper and include the following:

- KEY RESOURCES TABLE
- LEAD CONTACT AND MATERIALS AVAILABILITY
- EXPERIMENTAL MODEL AND SUBJECT DETAILS
  - Mice
  - Genotyping
  - OPN3 Mouse Lines
- METHOD DETAILS
  - Lighting Conditions
  - Intra-adipose Tissue Radiometry
  - Immunohistochemistry and Tissue Processing
  - X-Gal Staining
  - Hematoxylin Labeling and Cell-Size Quantification
  - Pre-Adipocyte Differentiation and Light Induction
  - Western Blotting
  - Glycerol Assay
  - Microarray Analysis
  - Quantitative RT-PCR
  - Transmission Electron Microscopy
  - NAD/NADH Quantification
  - Thermoregulation Assay
  - Indirect Calorimetry and Energy Expenditure
  - Tail Infrared Thermography (FLIR)
- QUANTIFICATION AND STATISTICAL ANALYSIS
- DATA AND CODE AVAILABILITY

SUPPLEMENTAL INFORMATION

Supplemental Information can be found online at https://doi.org/10.1016/j.celrep.2019.12.043.

ACKNOWLEDGMENTS

We thank Paul Speeg for excellent mouse colony management and the Transgenic Animal and Genome Editing Core at Cincinnati Children's Hospital. We thank Kwoon Y. Wong at the University of Michigan, Ann Arbor, for providing the *Opn4^{cre}; Z/EG* mouse line. This work was supported by NIH R01 GM124246 (to E.D.B.), R01EY026921 (to R.N.V.G.), P30EY001730 (to the University of Washington), R01 DK107530 (to T.N.), R01 EY027077 (to R.A.L. and S.R.), R01 EY027711 (to P. Michael Iuvone, Emory University, and R.A.L.); NIGMS T32 GM063483 (to the University of Cincinnati Medical Scientist Training Program); NIH P30 DK089503 (to R.J.S. and the Michigan Nutrition Obesity Research Center); the Mark J. Daily, MD Research Fund (to the University of Washington); and unrestricted grants to the University of Washington and Emory University Departments of Ophthalmology from Research to Prevent Blindness. This work was also supported by a Packard Foundation fellowship (to A.S.); American Heart Association grant 18CDA34080527 (to J.S.-G.); American Heart Association postdoctoral fellowship 19POST34380545 (to R.M.); and funds from the Goldman Chair of the Abrahamson Pediatric Eye Institute at Cincinnati Children's Hospital Medical Center.

AUTHOR CONTRIBUTIONS

G.N., K.X.Z., and S.V., experimental design and analysis and manuscript preparation. Y.O., E.D.B., A.H.-J., S.K., A.N.S., B.A.U., S.D., J.J.Z., N.D., M.-T.N., R.M., S.A.G., G.W., R.S., X.M., and S.R., experimental execution and analysis. N.T.P. and M.B., electronic device design and construction. J.B.H., supervision of bioinformatics analysis. R.J.S., T.N., A.S., R.N.V.G., J.S.-G., and R.A.L., project leadership, experimental design, and manuscript preparation.

DECLARATION OF INTERESTS

R.J.S. receives research support from Novo Nordisk, Zafgen, Kallyope, Pfizer, and Ironwood Pharmaceuticals.

Received: May 23, 2019
Revised: September 18, 2019
Accepted: December 12, 2019
Published: January 21, 2020

REFERENCES

Arimura, N., Horiba, T., Imagawa, M., Shimizu, M., and Sato, R. (2004). The peroxisome proliferator-activated receptor γ regulates expression of the perilipin gene in adipocytes. J. Biol. Chem. *279*, 10070–10076.

Barreto Ortiz, S., Hori, D., Nomura, Y., Yun, X., Jiang, H., Yong, H., Chen, J., Paek, S., Pandey, D., Sikka, G., et al. (2018). Opsin 3 and 4 mediate light-induced pulmonary vasorelaxation that is potentiated by G protein-coupled receptor kinase 2 inhibition. Am. J. Physiol. Lung Cell. Mol. Physiol. *314*, L93–L106.

Berry, R., Church, C.D., Gericke, M.T., Jeffery, E., Colman, L., and Rodeheffer, M.S. (2014). Imaging of adipose tissue. Methods Enzymol. *537*, 47–73.

Blackshaw, S., and Snyder, S.H. (1999). Encephalopsin: a novel mammalian extraretinal opsin discretely localized in the brain. J. Neurosci. *19*, 3681–3690.

Buhr, E.D., Yue, W.W.S., Ren, X., Jiang, Z., Liao, H.-W.R., Mei, X., Vemaraju, S., Nguyen, M.-T., Reed, R.R., Lang, R.A., et al. (2015). Neuropsin (OPN5)-mediated photoentrainment of local circadian oscillators in mammalian retina and cornea. Proc. Natl. Acad. Sci. USA *112*, 13093–13098.

Buhr, E.D., Vemaraju, S., Diaz, N., Lang, R.A., and Van Gelder, R.N. (2019). Neuropsin (OPN5) mediates local light-dependent induction of circadian clock genes and circadian photoentrainment in exposed murine skin. Curr. Biol. *29*, 3478–3487.e4.

Buscone, S., Mardaryev, A.N., Raafs, B., Bikker, J.W., Sticht, C., Gretz, N., Farjo, N., Uzunbajakava, N.E., and Botchkareva, N.V. (2017). A new path in defining light parameters for hair growth: Discovery and modulation of photoreceptors in human hair follicle. Lasers Surg. Med. *49*, 705–718.

Cajochen, C., Zeitzer, J.M., Czeisler, C.A., and Dijk, D.J. (2000). Dose-response relationship for light intensity and ocular and electroencephalographic correlates of human alertness. Behav. Brain Res. *115*, 75–83.

Cajochen, C., Münch, M., Kobialka, S., Kräuchi, K., Steiner, R., Oelhafen, P., Orgül, S., and Wirz-Justice, A. (2005). High sensitivity of human melatonin, alertness, thermoregulation, and heart rate to short wavelength light. J. Clin. Endocrinol. Metab. *90*, 1311–1316.

Cannon, B., and Nedergaard, J. (2004). Brown adipose tissue: function and physiological significance. Physiol. Rev. *84*, 277–359.

Carey, G.B. (1998). Mechanisms regulating adipocyte lipolysis. Adv. Exp. Med. Biol. *441*, 157–170.

Castellano-Pellicena, I., Uzunbajakava, N.E., Mignon, C., Raafs, B., Botchkarev, V.A., and Thornton, M.J. (2019). Does blue light restore human epidermal barrier function via activation of Opsin during cutaneous wound healing? Lasers Surg. Med. *51*, 370–382.

Cinti, S., Zingaretti, M.C., Cancello, R., Ceresi, E., and Ferrara, P. (2001). Morphologic techniques for the study of brown adipose tissue and white adipose tissue. Methods Mol. Biol. *155*, 21–51.

Cypess, A.M., Lehman, S., Williams, G., Tal, I., Rodman, D., Goldfine, A.B., Kuo, F.C., Palmer, E.L., Tseng, Y.-H., Doria, A., et al. (2009). Identification and importance of brown adipose tissue in adult humans. N. Engl. J. Med. *360*, 1509–1517.

Dijk, D.J., Cajochen, C., and Borbély, A.A. (1991). Effect of a single 3-hour exposure to bright light on core body temperature and sleep in humans. Neurosci. Lett. *121*, 59–62.

Divakaruni, A.S., and Brand, M.D. (2011). The regulation and physiology of mitochondrial proton leak. Physiology (Bethesda) *26*, 192–205.

Ecker, J.L., Dumitrescu, O.N., Wong, K.Y., Alam, N.M., Chen, S.K., LeGates, T., Renna, J.M., Prusky, G.T., Berson, D.M., and Hattar, S. (2010). Melanopsin-expressing retinal ganglion-cell photoreceptors: cellular diversity and role in pattern vision. Neuron *67*, 49–60.

Eguchi, J., Wang, X., Yu, S., Kershaw, E.E., Chiu, P.C., Dushay, J., Estall, J.L., Klein, U., Maratos-Flier, E., and Rosen, E.D. (2011). Transcriptional control of adipose lipid handling by IRF4. Cell Metab. *13*, 249–259.

Emig, D., Salomonis, N., Baumbach, J., Lengauer, T., Conklin, B.R., and Albrecht, M. (2010). AltAnalyze and DomainGraph: analyzing and visualizing exon expression data. Nucleic Acids Res. *38*, W755–W762.

Fan, W., and Evans, R. (2015). PPARs and ERRs: molecular mediators of mitochondrial metabolism. Curr. Opin. Cell Biol. *33*, 49–54.

Farley, F.W., Soriano, P., Steffen, L.S., and Dymecki, S.M. (2000). Widespread recombinase expression using FLPeR (flipper) mice. Genesis *28*, 106–110.

Fedorenko, A., Lishko, P.V., and Kirichok, Y. (2012). Mechanism of fatty-acid-dependent UCP1 uncoupling in brown fat mitochondria. Cell *151*, 400–413.

Fonken, L.K., and Nelson, R.J. (2014). The effects of light at night on circadian clocks and metabolism. Endocr. Rev. *35*, 648–670.

Fonken, L.K., Aubrecht, T.G., Meléndez-Fernández, O.H., Weil, Z.M., and Nelson, R.J. (2013). Dim light at night disrupts molecular circadian rhythms and increases body weight. J. Biol. Rhythms *28*, 262–271.

Giralt, M., and Villarroya, F. (2013). White, brown, beige/brite: different adipose cells for different functions? Endocrinology *154*, 2992–3000.

Gonzalez-Hurtado, E., Lee, J., Choi, J., and Wolfgang, M.J. (2018). Fatty acid oxidation is required for active and quiescent brown adipose tissue maintenance and thermogenic programing. Mol. Metab. *7*, 45–56.

Harms, M., and Seale, P. (2013). Brown and beige fat: development, function and therapeutic potential. Nat. Med. *19*, 1252–1263.

Hattar, S., Liao, H.W., Takao, M., Berson, D.M., and Yau, K.W. (2002). Melanopsin-containing retinal ganglion cells: architecture, projections, and intrinsic photosensitivity. Science *295*, 1065–1070.

Head, L.M., Tang, X., Hayley, S.E., Goda, T., Umezaki, Y., Chang, E.C., Leslie, J.R., Fujiwara, M., Garrity, P.A., and Hamada, F.N. (2015). The influence of light on temperature preference in *Drosophila*. Curr. Biol. *25*, 1063–1068.

Himms-Hagen, J. (1972). Lipid metabolism during cold-exposure and during cold-acclimation. Lipids *7*, 310–323.

Holt, A.L., Vahidinia, S., Gagnon, Y.L., Morse, D.E., and Sweeney, A.M. (2014). Photosymbiotic giant clams are transformers of solar flux. J. R. Soc. Interface *11*, 20140678.

Ikeda, K., Kang, Q., Yoneshiro, T., Camporez, J.P., Maki, H., Homma, M., Shinoda, K., Chen, Y., Lu, X., Maretich, P., et al. (2017). UCP1-independent signaling involving SERCA2b-mediated calcium cycling regulates beige fat thermogenesis and systemic glucose homeostasis. Nat. Med. *23*, 1454–1465.

Johnson, J., Wu, V., Donovan, M., Majumdar, S., Rentería, R.C., Porco, T., Van Gelder, R.N., and Copenhagen, D.R. (2010). Melanopsin-dependent light avoidance in neonatal mice. Proc. Natl. Acad. Sci. USA *107*, 17374–17378.

Kato, M., Sugiyama, T., Sakai, K., Yamashita, T., Fujita, H., Sato, K., Tomonari, S., Shichida, Y., and Ohuchi, H. (2016). Two Opsin 3-Related Proteins in the Chicken Retina and Brain: A TMT-Type Opsin 3 Is a Blue-Light Sensor in Retinal Horizontal Cells, Hypothalamus, and Cerebellum. PLoS ONE *11*, e0163925.

Kazak, L., Chouchani, E.T., Jedrychowski, M.P., Erickson, B.K., Shinoda, K., Cohen, P., Vetrivelan, R., Lu, G.Z., Laznik-Bogoslavski, D., Hasenfuss, S.C., et al. (2015). A creatine-driven substrate cycle enhances energy expenditure and thermogenesis in beige fat. Cell *163*, 643–655.

Kazak, L., Chouchani, E.T., Lu, G.Z., Jedrychowski, M.P., Bare, C.J., Mina, A.I., Kumari, M., Zhang, S., Vuckovic, I., Laznik-Bogoslavski, D., et al. (2017a). Genetic Depletion of Adipocyte Creatine Metabolism Inhibits Diet-Induced Thermogenesis and Drives Obesity. Cell Metab. *26*, 693.

Kazak, L., Chouchani, E.T., Stavrovskaya, I.G., Lu, G.Z., Jedrychowski, M.P., Egan, D.F., Kumari, M., Kong, X., Erickson, B.K., Szpyt, J., et al. (2017b). UCP1 deficiency causes brown fat respiratory chain depletion and sensitizes mitochondria to calcium overload-induced dysfunction. Proc. Natl. Acad. Sci. USA *114*, 7981–7986.

Klimova, L., Lachova, J., Machon, O., Sedlacek, R., and Kozmik, Z. (2013). Generation of mRx-Cre transgenic mouse line for efficient conditional gene deletion in early retinal progenitors. PLoS ONE *8*, e63029.

Kojima, D., and Fukada, Y. (1999). Non-visual photoreception by a variety of vertebrate opsins. Novartis Found. Symp. *224*, 265–279, discussion 279–282.

Kojima, D., Mori, S., Torii, M., Wada, A., Morishita, R., and Fukada, Y. (2011). UV-sensitive photoreceptor protein OPN5 in humans and mice. PLoS ONE *6*, e26388.

Kong, X., Banks, A., Liu, T., Kazak, L., Rao, R.R., Cohen, P., Wang, X., Yu, S., Lo, J.C., Tseng, Y.-H., et al. (2014). IRF4 is a key thermogenic transcriptional partner of PGC-1α. Cell *158*, 69–83.

Koyanagi, M., Takada, E., Nagata, T., Tsukamoto, H., and Terakita, A. (2013). Homologs of vertebrate Opn3 potentially serve as a light sensor in nonphotoreceptive tissue. Proc. Natl. Acad. Sci. USA *110*, 4998–5003.

Laermans, J., and Depoortere, I. (2016). Chronobesity: role of the circadian system in the obesity epidemic. Obes. Rev. *17*, 108–125.

Lakso, M., Pichel, J.G., Gorman, J.R., Sauer, B., Okamoto, Y., Lee, E., Alt, F.W., and Westphal, H. (1996). Efficient *in vivo* manipulation of mouse genomic sequences at the zygote stage. Proc. Natl. Acad. Sci. USA *93*, 5860–5865.

Langin, D., Holm, C., and Lafontan, M. (1996). Adipocyte hormone-sensitive lipase: a major regulator of lipid metabolism. Proc. Nutr. Soc. *55* (*1B*), 93–109.

Leone, T.C., Weinheimer, C.J., and Kelly, D.P. (1999). A critical role for the peroxisome proliferator-activated receptor alpha (PPARalpha) in the cellular fasting response: the PPARalpha-null mouse as a model of fatty acid oxidation disorders. Proc. Natl. Acad. Sci. USA *96*, 7473–7478.

Liu, C., Li, S., Liu, T., Borjigin, J., and Lin, J.D. (2007). Transcriptional coactivator PGC-1α integrates the mammalian clock and energy metabolism. Nature *447*, 477–481.

Liu, L., Zheng, L.D., Donnelly, S.R., Emont, M.P., Wu, J., and Cheng, Z. (2017). Isolation of Mouse Stromal Vascular Cells for Monolayer Culture. Methods Mol. Biol *1566*, 9–16.

Madisen, L., Zwingman, T.A., Sunkin, S.M., Oh, S.W., Zariwala, H.A., Gu, H., Ng, L.L., Palmiter, R.D., Hawrylycz, M.J., Jones, A.R., et al. (2010). A robust and high-throughput Cre reporting and characterization system for the whole mouse brain. Nat. Neurosci. *13*, 133–140.

Moriya, T., Miyashita, Y., Arai, J., Kusunoki, S., Abe, M., and Asami, K. (1996). Light-sensitive response in melanophores of *Xenopus laevis*: I. Spectral characteristics of melanophore response in isolated tail fin of *Xenopus* tadpole. J. Exp. Zool. *276*, 11–18.

Nakane, Y., Ikegami, K., Ono, H., Yamamoto, N., Yoshida, S., Hirunagi, K., Ebihara, S., Kubo, Y., and Yoshimura, T. (2010). A mammalian neural tissue opsin (Opsin 5) is a deep brain photoreceptor in birds. Proc. Natl. Acad. Sci. USA *107*, 15264–15268.

Nedergaard, J., Bengtsson, T., and Cannon, B. (2007). Unexpected evidence for active brown adipose tissue in adult humans. Am. J. Physiol. Endocrinol. Metab. *293*, E444–E452.

Nguyen, M.-T.T., Vemaraju, S., Nayak, G., Odaka, Y., Buhr, E.D., Alonzo, N., Tran, U., Batie, M., Upton, B.A., Darvas, M., et al. (2019). An opsin 5-dopamine pathway mediates light-dependent vascular development in the eye. Nat. Cell Biol. *21*, 420–429.

Nissilä, J., Mänttäri, S., Särkioja, T., Tuominen, H., Takala, T., Timonen, M., and Saarela, S. (2012). Encephalopsin (OPN3) protein abundance in the adult mouse brain. J. Comp. Physiol. A Neuroethol. Sens. Neural Behav. Physiol. *198*, 833–839.

Okano, T., Yoshizawa, T., and Fukada, Y. (1994). Pinopsin is a chicken pineal photoreceptive molecule. Nature *372*, 94–97.

Olivecrona, G. (2016). Role of lipoprotein lipase in lipid metabolism. Curr. Opin. Lipidol. *27*, 233–241.

Ondrusova, K., Fatehi, M., Barr, A., Czarnecka, Z., Long, W., Suzuki, K., Campbell, S., Philippaert, K., Hubert, M., Tredget, E., et al. (2017). Subcutaneous white adipocytes express a light sensitive signaling pathway mediated via a melanopsin/TRPC channel axis. Sci. Rep. *7*, 16332.

Opperhuizen, A.L., Stenvers, D.J., Jansen, R.D., Foppen, E., Fliers, E., and Kalsbeek, A. (2017). Light at night acutely impairs glucose tolerance in a time-, intensity- and wavelength-dependent manner in rats. Diabetologia *60*, 1333–1343.

Panda, S., Sato, T.K., Castrucci, A.M., Rollag, M.D., DeGrip, W.J., Hogenesch, J.B., Provencio, I., and Kay, S.A. (2002). Melanopsin (*Opn4*) requirement for normal light-induced circadian phase shifting. Science *298*, 2213–2216.

Panda, S., Provencio, I., Tu, D.C., Pires, S.S., Rollag, M.D., Castrucci, A.M., Pletcher, M.T., Sato, T.K., Wiltshire, T., Andahazy, M., et al. (2003). Melanopsin is required for non-image-forming photic responses in blind mice. Science *301*, 525–527.

Peek, C.B., Affinati, A.H., Ramsey, K.M., Kuo, H.Y., Yu, W., Sena, L.A., Ilkayeva, O., Marcheva, B., Kobayashi, Y., Omura, C., et al. (2013). Circadian clock NAD+ cycle drives mitochondrial oxidative metabolism in mice. Science *342*, 1243417.

Provencio, I., Jiang, G., De Grip, W.J., Hayes, W.P., and Rollag, M.D. (1998). Melanopsin: An opsin in melanophores, brain, and eye. Proc. Natl. Acad. Sci. USA *95*, 340–345.

Puigserver, P., Wu, Z., Park, C.W., Graves, R., Wright, M., and Spiegelman, B.M. (1998). A cold-inducible coactivator of nuclear receptors linked to adaptive thermogenesis. Cell *92*, 829–839.

Rao, S., Chun, C., Fan, J., Kofron, J.M., Yang, M.B., Hegde, R.S., Ferrara, N., Copenhagen, D.R., and Lang, R.A. (2013). A direct and melanopsin-dependent fetal light response regulates mouse eye development. Nature *494*, 243–246.

Regard, J.B., Sato, I.T., and Coughlin, S.R. (2008). Anatomical profiling of G protein-coupled receptor expression. Cell *135*, 561–571.

Regazzetti, C., Sormani, L., Debayle, D., Bernerd, F., Tulic, M.K., De Donatis, G.M., Chignon-Sicard, B., Rocchi, S., and Passeron, T. (2018). Melanocytes Sense Blue Light and Regulate Pigmentation through Opsin-3. J. Invest. Dermatol. *138*, 171–178.

Rhee, J., Inoue, Y., Yoon, J.C., Puigserver, P., Fan, M., Gonzalez, F.J., and Spiegelman, B.M. (2003). Regulation of hepatic fasting response by PPARgamma coactivator-1alpha (PGC-1): requirement for hepatocyte nuclear factor 4alpha in gluconeogenesis. Proc. Natl. Acad. Sci. USA *100*, 4012–4017.

Rogne, M., and Taskén, K. (2014). Compartmentalization of cAMP signaling in adipogenesis, lipogenesis, and lipolysis. Horm. Metab. Res. *46*, 833–840.

Rosenwald, M., Perdikari, A., Rülicke, T., and Wolfrum, C. (2013). Bi-directional interconversion of brite and white adipocytes. Nat. Cell Biol. *15*, 659–667.

Rupp, A.C., Ren, M., Altimus, C.M., Fernandez, D.C., Richardson, M., Turek, F., Hattar, S., and Schmidt, T.M. (2019). Distinct ipRGC subpopulations mediate light's acute and circadian effects on body temperature and sleep. eLife *8*, e44358.

Sakami, S., Maeda, T., Bereta, G., Okano, K., Golczak, M., Sumaroka, A., Roman, A.J., Cideciyan, A.V., Jacobson, S.G., and Palczewski, K. (2011). Probing mechanisms of photoreceptor degeneration in a new mouse model of the common form of autosomal dominant retinitis pigmentosa due to P23H opsin mutations. J. Biol. Chem. *286*, 10551–10567.

Salomonis, N. (2012). AltAnalyze—An optimized platform for RNA-seq splicing and domain-level analyses. In Proceedings of the 2012 IEEE 2nd Conference on Healthcare Informatics, Imaging and Systems Biology (IEEE), p. 113.

Sanchez-Gurmaches, J., Hung, C.-M., Sparks, C.A., Tang, Y., Li, H., and Guertin, D.A. (2012). PTEN loss in the Myf5 lineage redistributes body fat and reveals subsets of white adipocytes that arise from Myf5 precursors. Cell Metab. *16*, 348–362.

Sato, K., Yamashita, T., Haruki, Y., Ohuchi, H., Kinoshita, M., and Shichida, Y. (2016). Two UV-sensitive photoreceptor proteins, Opn5m and Opn5m2 in rayfinned fish with distinct molecular properties and broad distribution in the retina and brain. PLoS ONE *11*, e0155339.

Schreiber, R., Diwoky, C., Schoiswohl, G., Feiler, U., Wongsiriroj, N., Abdellatif, M., Kolb, D., Hoeks, J., Kershaw, E.E., Sedej, S., et al. (2017). Cold-Induced Thermogenesis Depends on ATGL-Mediated Lipolysis in Cardiac Muscle, but Not Brown Adipose Tissue. Cell Metab. *26*, 753–763.e7.

Seale, P. (2013). Brown adipose tissue biology and therapeutic potential. Front. Endocrinol. (Lausanne) *4*, 14.

Shabalina, I.G., Petrovic, N., de Jong, J.M.A., Kalinovich, A.V., Cannon, B., and Nedergaard, J. (2013). UCP1 in brite/beige adipose tissue mitochondria is functionally thermogenic. Cell Rep. *5*, 1196–1203.

Shin, H., Ma, Y., Chanturiya, T., Cao, Q., Wang, Y., Kadegowda, A.K.G., Jackson, R., Rumore, D., Xue, B., Shi, H., et al. (2017). Lipolysis in Brown Adipocytes Is Not Essential for Cold-Induced Thermogenesis in Mice. Cell Metab. *26*, 764–777.e5.

Shin, H., Shi, H., Xue, B., and Yu, L. (2018). What activates thermogenesis when lipid droplet lipolysis is absent in brown adipocytes? Adipocyte *7*, 143–147.

Sikka, G., Hussmann, G.P., Pandey, D., Cao, S., Hori, D., Park, J.T., Steppan, J., Kim, J.H., Barodka, V., Myers, A.C., et al. (2014). Melanopsin mediates light-dependent relaxation in blood vessels. Proc. Natl. Acad. Sci. USA *111*, 17977–17982.

Sikka, G., Hori, D., Pandey, D., Barreto, S., and Berkowitz, D. (2016). Opsin 3 and 4 mediate light-dependent vasorelaxation: Therapeutic targets in pulmonary hypertension. Crit. Care Med. *44*, 138.

Syamsunarno, M.R.A.A., Iso, T., Yamaguchi, A., Hanaoka, H., Putri, M., Obokata, M., Sunaga, H., Koitabashi, N., Matsui, H., Maeda, K., et al. (2014). Fatty acid binding protein 4 and 5 play a crucial role in thermogenesis under the conditions of fasting and cold stress. PLoS ONE *9*, e90825.

van Marken Lichtenbelt, W.D., Vanhommerig, J.W., Smulders, N.M., Drossaerts, J.M.A.F.L., Kemerink, G.J., Bouvy, N.D., Schrauwen, P., and Teule, G.J.J. (2009). Cold-activated brown adipose tissue in healthy men. N. Engl. J. Med. *360*, 1500–1508.

Vega, R.B., Huss, J.M., and Kelly, D.P. (2000). The coactivator PGC-1 cooperates with peroxisome proliferator-activated receptor alpha in transcriptional control of nuclear genes encoding mitochondrial fatty acid oxidation enzymes. Mol. Cell. Biol. *20*, 1868–1876.

Virtanen, K.A., Lidell, M.E., Orava, J., Heglind, M., Westergren, R., Niemi, T., Taittonen, M., Laine, J., Savisto, N.-J., Enerbäck, S., and Nuutila, P. (2009). Functional brown adipose tissue in healthy adults. N. Engl. J. Med. *360*, 1518–1525.

Wong, K.Y. (2012). A retinal ganglion cell that can signal irradiance continuously for 10 hours. J. Neurosci. *32*, 11478–11485.

Wu, J., Boström, P., Sparks, L.M., Ye, L., Choi, J.H., Giang, A.-H., Khandekar, M., Virtanen, K.A., Nuutila, P., Schaart, G., et al. (2012). Beige adipocytes are a distinct type of thermogenic fat cell in mouse and human. Cell *150*, 366–376.

Xue, B., Rim, J.-S., Hogan, J.C., Coulter, A.A., Koza, R.A., and Kozak, L.P. (2007). Genetic variability affects the development of brown adipocytes in white fat but not in interscapular brown fat. J. Lipid Res. *48*, 41–51.

Yamashita, T., Ohuchi, H., Tomonari, S., Ikeda, K., Sakai, K., and Shichida, Y. (2010). Opn5 is a UV-sensitive bistable pigment that couples with Gi subtype of G protein. Proc. Natl. Acad. Sci. USA *107*, 22084–22089.

Yoshimoto, T., Morine, Y., Takasu, C., Feng, R., Ikemoto, T., Yoshikawa, K., Iwahashi, S., Saito, Y., Kashihara, H., Akutagawa, M., et al. (2018). Blue light-emitting diodes induce autophagy in colon cancer cells by Opsin 3. Ann. Gastroenterol. Surg. *2*, 154–161.

Zechner, R., Zimmermann, R., Eichmann, T.O., Kohlwein, S.D., Haemmerle, G., Lass, A., and Madeo, F. (2012). FAT SIGNALS—lipases and lipolysis in lipid metabolism and signaling. Cell Metab. *15*, 279–291.

STAR★METHODS

KEY RESOURCES TABLE

REAGENT or RESOURCE	SOURCE	IDENTIFIER
Antibodies		
Rabbit polyclonal anti-UCP1	Abcam	ab10983; RRID: AB_2241462
Chicken polyclonal anti-GFP	Abcam	ab13970; RRID: AB_330798
Rabbit polyclonal anti-TUBB3	BioLegend	802001; RRID: AB_2564645
Rabbit polyclonal anti-Recoverin	Millipore Sigma	AB5585; RRID: AB_2253622
Phalloidin (Alexa Fluor 594)	Thermo Fisher Scientific	A12381; RRID: AB_2315633
Mouse monoclonal anti-Rhodopsin	Abcam	ab3267; RRID: AB_303655
Isolectin IB4 (Alexa Fluor 488)	Thermo Fisher Scientific	I21411; RRID: AB_2314662
Anti-Phospho-PKA (pThr197)	Cell Signaling Technology	5661S; RRID: AB_10707163
Anti-PKA C-a	Cell Signaling Technology	5842S; RRID: AB_10706172
Anti-Phospho-PKA Substrate (RRxpS/T)	Cell Signaling Technology	9624S; RRID: AB_331817
Anti-Phospho-HSL (pSer660)	Cell Signaling Technology	4126S; RRID: AB_490997
Anti-HSL	Cell Signaling Technology	18381T; RRID: AB_2798800
Anti-Phospho-PLIN1 (pSer522)	Vala Sciences	4856
Anti-Phospho-CREB (pSer133)	Cell Signaling Technology	9198S; RRID: AB_2561044
Anti-phospho-ERK (p44/42)	Cell Signaling Technology	9102S; RRID: AB_330744
Chemicals, Peptides, and Recombinant Proteins		
DMEM High Glucose	Thermo Fisher Scientific	11965-092
Insulin	Millipore Sigma	I2643
Rosiglitazone	Millipore Sigma	R2408
Dexamethasone	Millipore Sigma	D1756
IBMX	Millipore Sigma	I5879
9-*cis*-Retinal	Millipore Sigma	R5754
Critical Commercial Assays		
cAMP Assay Kit (Competitive ELISA, Fluorometric)	Abcam	ab138880
OxPhos Rodent WB Antibody Cocktail	Thermo Fisher Scientific	45-8099; RRID: AB_2533835
Free Glycerol Reagent	Millipore Sigma	F6428
GeneJET RNA Purification Kit	Thermo Fisher Scientific	K0732
Verso cDNA Synthesis Kit	Thermo Fisher Scientific	AB1453
NAD/NADH Assay Kit (Colorimetric)	Abcam	ab65348
Deposited Data		
Gene Expression Dataset	GEO NCBI	GEO: GSE140757
Experimental Models: Organisms/Strains		
Mouse: *Adipoq-cre: B6.FVB-Tg$^{(Adipoq-cre)1Evdr}$/J*	The Jackson Laboratory	010803; RRID: IMSR_JAX:010803
Mouse: *Ucp1-cre: B6.FVB-Tg$^{(Ucp1-cre)1Evdr}$/J*	The Jackson Laboratory	024670; RRID: IMSR_JAX:024670
Mouse: *Ai14: B6;129S6-Gt(ROSA)26Sor$^{tm14(CAG-tdTomato)Hze}$/J*	The Jackson Laboratory	007908; RRID: IMSR_JAX:007908
Mouse: *Opn2: B6.129S6(Cg)-Rho$^{tm1.1Kpal}$/J*	The Jackson Laboratory	017628; RRID: IMSR_JAX:017628
Mouse: *C57BL/6J*	The Jackson Laboratory	000664; RRID: IMSR_JAX:000664
Mouse: *Rx-cre: B6.Cg-Tg$^{(Rax-cre)1Zkoz/Ph}$/J*	Klimova et al., 2013	N/A
Mouse: *Opn3$^{lacZ/lacZ}$*	This paper	N/A
Mouse: *Opn3$^{fl/fl}$*	This paper	N/A
Mouse: *Opn3$^{\Delta Ex2/\Delta Ex2}$*	This paper	N/A
Mouse: *Opn3^{cre}*	This paper	N/A
Mouse: *Opn3-eGFP: B6-Tg$^{(Opn3-EGFPJY3Gsat/Mmucd)}$/J*	GENSAT	030727-UCD; RRID: MMRRC_030727-UCD

(*Continued on next page*)

Continued		
REAGENT or RESOURCE	SOURCE	IDENTIFIER
Mouse: *Opn4: Opn4*^{tm1Skay}	KOMP Repository	MGI: 2449695
Mouse: *Opn3: Opn3*$^{tm2a(EUCOMM)Wtsi}$	EuMMCR Repository	MGI: 4434308
Mouse: *Opn4*^{cre}*; Z/EG*	Ecker et al., 2010	N/A
Oligonucleotides		
Dio2 F: CAGTGTGGTGCACGTCTCCAATC	This Paper	N/A
Dio2 R: TGAACCAAAGTTGACCACCAG	This Paper	N/A
Prdm16 F: CAGCACGGTGAAGCCATTC	This Paper	N/A
Prdm16 R: GCGTGCATCCGCTTGTG	This Paper	N/A
Pgc1α F: CCCTGCCATTGTTAAGACC	This Paper	N/A
Pgc1α R: TGCTGCTGTTCCTGTTTTC	This Paper	N/A
Cidea F: TGCTCTTCTGTATCGCCCAGT	This Paper	N/A
Cidea R: GCCGTGTTAAGGAATCTGCTG	This Paper	N/A
Ucp1 F: ACTGCCACACCTCCAGTCATT	This Paper	N/A
Ucp1 R: CTTTGCCTCACTCAGGATTGG	This Paper	N/A
Pparγ F: GTGCCAGTTTCGATCCGTAGA	This Paper	N/A
Pparγ R: GGCCAGCATCGTGTAGATGA	This Paper	N/A
Hprt1 F: TCAGTCAACGGGGGACATAAA	This Paper	N/A
Hprt1 R: GGGGCTGTACTGCTTAACCAG	This Paper	N/A
Tbp F: GAAGCTGCGGTACAATTCCAG	This Paper	N/A
Tbp R: CCCCTTGTACCCTTCACCAAT	This Paper	N/A
Software and Algorithms		
GraphPad Prism 8.2.1	GraphPad	GraphPad.com
MATLAB 2018a	Mathworks	Mathworks.com
ImageJ/Fiji 2.0.0	ImageJ	ImageJ.nih.gov
AltAnalyze	Salomonis, 2012	AltAnalyze.org
FLIR Tools Version 2.1	FLIR	Flir.com
Other		
Infrared Thermal Camera	FLIR	T530
Rectal Thermometer Probe	Physitemp	RET-3
TSE PhenoMaster	TSE Systems Inc.	N/A
JAZ Spectrometer	Ocean Optics	JAZ

LEAD CONTACT AND MATERIALS AVAILABILITY

This study did not generate new unique reagents. Mouse lines generated in this study are available from the Lead Contact with a completed Materials Transfer Agreement. Further information and request for resources should be directed to and will be fulfilled by the Lead Contact, Richard A. Lang (richard.lang@cchmc.org).

EXPERIMENTAL MODEL AND SUBJECT DETAILS

All experiments were approved by Cincinnati Children's Hospital Medical Center, The University of Michigan Ann Arbor, and The University of Washington Institutional Animal Care and Use Committees and were in accordance with the National Institute of Health guidelines. Ages of mice used in this study include P16 (immunohistochemical analyses and microarray), P21-P24 (neonatal cold exposure), P28 (transmission electron microscopy), 2 months (adult cold exposure), and 3-4 months (fiber radiometry and indirect calorimetry). Male and female mice were used for all studies unless otherwise stated.

Mice

Animals were housed in a pathogen-free vivarium in accordance with institutional policies. Genetically modified mice used in this study were: *B6;FVB-Tg(Adipoq-cre)1Evdr/J* (Eguchi et al., 2011)(Jax stock #010803), *Ai14* (Madisen et al., 2010)(Jax stock #007914), *Opn4* (Panda et al., 2003), and *Tg(Opn3-EGFP)JY3Gsat* (MMRRC stock number 030727-UCD). The *Ucp1*^{cre} mouse line

used in the thermoregulation assay studies was obtained from Jackson Laboratories: *B6.FVB-Tg(Ucp1-cre)1Evdr/J* (Jax stock #024670). The *Opn4^{cre}; Z/EG* mouse line was generously donated by Kwoon Y. Wong from the University of Michigan Ann Arbor (Ecker et al., 2010). *Opn3$^{tm2a(EUCOMM)Wtsi}$* mice were generated from C57BL/6N ES cells obtained from EUCOMM (ES clone ID: EPD0197_3_E01). The ES cells harbor a genetic modification wherein the lacz-Neomycin cassette is flanked by FRT sites and a *loxp* site separates lacz from the neomycin coding region. *Loxp* sites also flank exon 2 of *Opn3* allowing multiple mouse lines that can serve as reporter nulls, conditional floxed and null mice. The *Opn3^{Lacz}* reporter null line was created by crossing *Opn3$^{tm2a(EUCOMM)Wtsi}$* mice to *FVB/N-Tg(EIIa-cre)C5379Lmgd/J* mice (Lakso et al., 1996)(Jax stock #003314). *Opn3$^{fl/fl}$* line was created by crossing the *Opn3$^{tm2a(EUCOMM)Wtsi}$* mice to *129S4/SvJaeSor-Gt(ROSA)26Sor$^{tm1(FLP1)Dym}$/J*(Farley et al., 2000)(Jax stock #003946) to remove the *lacZ* cassette. This means that *Opn3^{lacz}* mice are of mixed C57Bl6/6N, FVB/N background and that *Adipoq-cre; Opn3^{fl}* mice are of mixed C57Bl6/6N, 129S4/Sv, B6;FVB background. Littermate control animals were used for all experiments with the exception of C57BL/6J mice reared under different lighting conditions.

The *Opn3^{cre}* was generated in-house using CRISPR-Cas9 technology. Four gRNAs that target exon 2 of *Opn3* were selected to knock in the Cre cassette. Plasmids containing the gRNA sequence were transfected into MK4 cells (an in-house mouse cell line representing induced metanephric mesenchyme undergoing epithelial conversion). The editing efficiency of gRNA was determined by T7E1 assay of PCR products of the target region amplified from genomic DNA of transfected MK4 cells. The sequence of the gRNA that was subsequently used for the transfection is TACCGTGGACTGGAGATCCA. Sanger sequencing was performed to validate the knock-in sequence of founder mice.

The *Opn3ΔEx2* allele was generated in-house using CRISPR-Cas9 technology as above. Four gRNAs that target exon 2 of *Opn3* were selected. The sequences of the gRNAs are: for the 5′ end: TAGCAACGAATGCAAAGGTA GGG and ATCCACATGTTCTGCC CAGGAGG. For the 3′ end: GCGCTATGTTGGTAAGGTGT GGG and TGTGGTTTTAATCAGCACAGGGG. Out of the 6 pups derived from one injection, the founder animal had a 2203 bp deletion that was also confirmed by Sanger sequencing. The proximal breakpoint of this deletion is intron 1 (bp 175,667,424) to intron 2 (bp175,665,054) thus deleting the entirety of exon 2.

Mice were placed on normal chow diet (NCD: 29% Protein, 13% Fat and 58% Carbohydrate kcal; LAB Diet #5010) *ad libitum* with free access to water.

Genotyping

Primer sequences and pairs for genotyping each of the alleles in this study are listed in the table below:

Allele	Primers	Pairs	bp
Opn3	F1: ACCCAGGCTTCTTTTGGTCT	F1R1 – Wild-type	1191
	R1: AGAGTCGTTGGCATCCTTGG	F1R1 – *Opn3^{fl}*	1231
	F2: ACTATCCCGACCGCCTTACT	F1R2 – *Opn3^{fl}*	1610
	R2: GAACTGATGGCGAGCTCAGA	F1R2 – *Opn3^{cko}*	640
		F2R2 – *Opn3^{lacz}*	701
Opn3^{cre}	F1: TGCTGGCCTATGAACGTTATATCC	F1R1 – Wild-type	401
	R1: TCAGTTCTGGGTGACTAACTGATC	F1R2 – *Opn3^{cre}*	390
	R2: CACTCGTTGCATCGACCGGTAATGC		
Adipoq^{cre}	F: GCATTACCGGTCGATGCAACGAGTGATGAG	FR – *cre*	450
Ucp1^{cre}	R: GAGTGAACGAACCTGGTCGAAATCAGTGCG		
Rx^{cre}			
Opn3^{ΔEx2}	F1: CTCAGAACCCACAAAGTGCTGG	F1R1 – Wild-type	307
	R1: GTGGACTGCAATGTCCCATCTATC	F1R2 – *Opn3^{ΔEx2}*	191
	R2: GTGGGCATCATAGCCCATTGCTAC		
Opn4	F1: AGGAGTGTATAGAGCCGGAAGTCTG	F1R1 – Wild-type	520
	R1: CCAGTCCAGAAGCCTAGGGCATGCC	F2R2 – *Opn4^{-}*	380
	F2: TGCTCCTGCCGAGTATCCATCATGGC		
	R2: CGCCAAGCTCTTCATATCACGGGTAG		
Opn4^{cre}	F1: AGGCTGGATGGATGAGAGC	F1R1 – Wild-type	187
	R1: GTTGTGAAGCTGGGATCCTG	F2R2 – *cre*	184
	F2: CGACCAGGTTCGTTCACTCA		
	R2: CAGCGTTTTCGTTCTGCCAA		
Z/EG	F: CCCCTGCTGTCCATTCCTTA	FR – *Z/EG*	224
	R: TGACCATGATTACGCAAGC		

OPN3 Mouse Lines

All OPN3 mouse lines used in this study, along with the scientific rationale, are detailed in the table below:

Allele	Mouse Lines	Rationale & Data
Opn3^{lKMC}		Parent allele used to derive other modular alleles.
Opn3^{lacZ}	*Opn3*$^{lacZ/lacZ}$	Reporter null allele. Key data presented for this mouse line includes Figures 1, 3, 4, 6, and 7, where we show adipocyte expression, adipocyte morphometric differences, NAD, ETC, body temperature, gene expression differences, and adipocyte specific light responses.
Opn3^{fl}	*Adipoq*^{cre}; *Opn3*$^{fl/fl}$	Conditional deletion of *Opn3* from adipocytes. Key data for this mouse line are presented in Figures 5 and 7 where we directly measure markers of lipolysis that are OPN3- and light-dependent. This allele is crucial because it permits us to focus on analyses that explore adipocyte-specific OPN3 functions. Additional data on tail temperature from *Opn3*$^{fl/fl}$ and *Adipoq*^{cre}; *Opn3*$^{fl/fl}$ animals are presented in Figure S5C.
	Ucp1^{cre}; *Opn3*$^{fl/fl}$	Conditional deletion of *Opn3* from brown adipocytes. Key data for this mouse line are presented in Figure 5E showing no difference between *Opn3*$^{fl/fl}$ and *Ucp1*^{cre}; *Opn3*$^{fl/fl}$ adult mice in defended body temperature following cold exposure.
	Rx^{cre}; *Opn3*$^{fl/fl}$	Conditional deletion of *Opn3* from retinal progenitors. Key data for this mouse line are presented in Figure S5B showing no difference in defended core body temperature between cold exposed *Opn3*$^{fl/fl}$ and *Rx*^{cre}; *Opn3*$^{fl/fl}$ adult mice.
Opn3^{cre}	*Opn3*^{cre}; *Ai14*	In house developed and validated constitutive *Cre* driver line used in combination with *Ai14* (Jax #007908) to characterize OPN3 expression in iscWAT and iBAT via the fluorescent *tdTomato* reporter. Key data presented for this line are in Figures 1I–1K.
Opn3$^{\Delta Ex2}$	*Opn3*$^{\Delta Ex2/\Delta Ex2}$	In house generated CRISPR-Cas9 mediated 2203 bp deletion of exon 2 of the *Opn3* locus. Key data presented for this mouse line is in Figure 4B, showing persistence of defended core body temperature differences between controls and *Opn3* loss-of-function animals on a congenic C57BL/6J background.

METHOD DETAILS

Lighting Conditions

Animals were housed in standard fluorescent lighting (photon flux 1.62x10^{15} photons/cm^2/sec) on a 12L:12D cycle except where noted. For full spectrum lighting, LEDs were used to yield a comparable total photon flux of 1.68 × 10^{15} photons/cm^2/sec. Spectral and photon flux information for LED lighting: near violet (λ_{max} = 380 nm, 4.23 × 10^{14} photons/cm^2/sec in the 370-400 nm range), blue (λ_{max} = 480 nm, 5.36 × 10^{14} photons/cm^2/sec in the 430-530 nm range), and red (λ_{max} = 630 nm, 6.72 × 10^{14} photons/cm^2/sec in the 590-660 nm range). Photon fluxes were measured at approximately 24'' from source and through an empty standard mouse cage. For wavelength restricted experiments, C57BL/6J animals were housed in a 12L:12D cycle starting late gestation (embryonic day E16) either in full spectrum (380 nm + 480 nm + 630 nm LEDs) or in ''minus blue'' (380 nm + 630 nm LEDs) lighting.

Intra-adipose Tissue Radiometry

Fabrication of the Holt-Sweeney microprobe (HSM) is described as follows (Holt et al., 2014). The termination of one end of a 100 μm silica core fiber optic patch cable (Ocean Optics, Dunedin, FL, USA) was removed. The fiber's furcation tubing and jacketing was stripped, and the fiber's polyimide buffer was removed 5 cm from the fiber's end using a butane torch. A 10 g weight was attached to the end of the fiber and then pulled upon heating with the butane torch, narrowing the diameter. The narrowed region of the fiber was then cut using carborundum paper, to yield a flat fiber end with a diameter of 30 – 50 μm. The sides of the narrowed fiber were painted with a film opaquing pen to prevent stray light from entering, while leaving a small transparent opening at the fiber tip. For structural support, this bare, tapered fiber was then secured in the tip of a pulled glass Pasteur pipette using a drop of cyanoacrylate glue, leaving only 6-9 mm of bare optical fiber protruding. A small light-scattering ball was added to the end of the tapered optical fiber for spectral scalar irradiance measurements. To do this, titanium dioxide was thoroughly mixed with a high-viscosity UV-curable resin, DELO-PHOTOBOND, GB368 (DELO Industrie Klebstoffe, Windach, Germany). The tip of a pulled fiber was quickly inserted and removed from a droplet of the resin and titanium dioxide mixture, resulting in a sphere with a diameter of approximately twice that of the tapered fiber. As all measurements from a given probe were normalized to the signal from the same probe in a gelatin blank, small variations in the probe diameter have no effect on our results. The sphere was cured for 12 h using a Thorlabs fiber coupled LED light source (M375F2, Thorlabs Inc, Newton, NJ, USA).

For intra-tissue radiometric measurements in mice, 4 month-old adult animals were anesthetized under ventilated isoflurane and placed in a mouse stereotaxic frame (Stoelting Co, Wood Dale, IL, USA). The hair overlying the intrascapular region was shaved and a

small 10 mm rostrocaudal incision was made through the dorsal skin to expose the underlying tissue. A 21-gauge needle attached to the stereotaxic frame was first lowered through the intrascapular region to produce a pilot hole through the adipose tissue. Following, the Holt-Sweeney microprobe was affixed to the stereotaxic frame and lowered through the pilot hole. After the probe is in position, the dorsal skin was repositioned to cover as much of the incision site as possible without obstructing the probe's descent. For broad-band light illumination, a Thorlabs plasma light source (HPLS345, Thorlabs Inc, Newton, NJ, USA) was positioned above and in front of the mouse stereotaxic frame. The light was delivered to the animal via a 5 mm liquid light guide connected to a 2 in. collimating lens secured in a vice. The distance from the collimating lens to the animal was approximately 2 ft.

Scalar irradiance measurements as a function of wavelength were obtained at the surface of the adipose tissue and at probe depth increments of 0.5 mm up to 2.5 mm. Spectral irradiance data were collected using an Ocean Optics 200-850 nm spectrometer (JAZ series, Ocean Optics, Dunedin, FL, USA).

Immunohistochemistry and Tissue Processing

Animals were anesthetized under isoflurane and sacrificed by cervical dislocation. Adipose tissue depots (interscapular adipose tissue complex and inguinal WAT) from P16 male mice were harvested and fixed in ice cold 10% zinc formalin for 1 hour at 4°C. After washing in PBS, adipose tissue samples were prepared for cryosectioning as described previously (Berry et al., 2014). Gelatin-embedded tissues were sectioned at 16 μm in a cryostat and labeled with primary antibodies as previously described (Berry et al., 2014). Chicken antibodies to GFP (ab13970, 1 in 500), and rabbit antibodies to UCP1 (ab10983, 1 in 500), were purchased from Abcam. Alexa 488 conjugated isolectin (1 in 300) and Alexa 594 conjugated F-actin were purchased from Thermo Fisher Scientific. Alexa 488 conjugated secondary antibodies (1 in 300) were purchased from Jackson ImmunoResearch.

X-Gal Staining

For X-Gal labeling, tissue samples were fixed in X-Gal fixative (1% formaldehyde, 0.2% glutaraldehyde, 2 mM $MgCl_2$, 5 mM EGTA, and 0.01% Nonidet P-40) for two hours at room temperature. Tissues were cryosectioned as described above and then labeled with X-Gal. The reaction was monitored closely and stopped when background started to appear in control (wild-type) tissues. Following two washes in PBS, cryosections were imaged using a bright field microscope.

Hematoxylin Labeling and Cell-Size Quantification

Gelatin-embedded frozen sections of inguinal WAT (as described above) were stained with hematoxylin and imaged under bright-field. Samples were imaged with a rhodamine filter to assess adipocyte size distribution. Using the free hand selection tool on ImageJ, adipocytes were outlined and the area measured in μm^2. Cell size distribution was determined by quantifying 60 cells from at least 10 regions, for a total of approximately 600 cells per animal. Cell areas were binned into 200 μm^2 intervals and the frequency of total cells (%) charted for each interval.

Pre-Adipocyte Differentiation and Light Induction

IngWAT dissociation and extraction of stromal vascular fraction was performed as described before (Liu et al., 2017). Briefly, the inguinal fat pads were collected in PBS and digested in 1.5 mg/ml Collagenase A in PBS with 4% BSA and penicillin/streptomycin at 37°C, with intermittent agitation over 40 minutes. The stromal vascular fraction was extracted by passing the enzymatically dispersed cells through a 100 μm cell strainer and cultured in basal media (DMEM containing 10% fetal bovine serum and penicillin/streptomycin). For differentiation, the stromal vascular cells were plated on day1 such that the cells reached confluency on day 3. On day 4, the basal media was replaced with induction media containing Insulin (100 nM), Rosiglitazone (1 μM), IBMX (0.5 mM) and Dexamethasone (2 μg/ml) in basal media. Thereafter, the differentiating cells were maintained in basal media containing insulin (100 nM) until the day of experimentation.

Light inductions to assay lipolysis responses were typically done on day 13 – day 15 of differentiation. For this, cultures were moved to a dark, 37°C incubator, protected from light, overnight. The next day, the cultures were serum-starved, under dim red light, where the complete basal medium was washed out using serum-free medium (at least three washes) and the cells were left in serum-free media for 3 hours, before light inductions. For light inductions, half the *Opn3*$^{+/+}$ and *Opn3*$^{Lacz/Lacz}$ cultures were left in the dark incubator, while the rest were moved to an adjacent incubator that housed a light set-up to deliver $5x10^{14}$ photons/cm^2/sec of 480 nm wavelength. The culture conditions in the two incubators were comparable except for the lighting. Prior to stimulation, any movement between incubators was accomplished with care and within a matter of seconds so as to avoid any potential temperature shock. Wild-type controls were always processed alongside *Opn3* null samples. Light inductions were carried out for 30 minutes, after which the cells were washed in PBS and snap frozen by immersing the culture plates in liquid nitrogen and frozen at −80°C until lysate preparations for western blotting.

@For the light-induced cyclic AMP response, *in vitro* differentiated *Opn3*$^{+/+}$ and *Opn3*$^{Lacz/Lacz}$ adipocytes were used between days 7 and 10 of differentiation. The cells were incubated with 9-cis-Retinal (5 μM) the day before the assay and one hour before the light induction, the cells were incubated in fresh DMEM without phenol red. The light pulses (465 nm) were delivered for 30 minutes with varying intensities as indicated in the results. The cells were then harvested to quantify cAMP levels by direct immunoassay (fluorometric kit by Abcam, ab138880) as per manufacturer's instructions. For *ex vivo* cAMP quantification from harvested tissue, dissected inguinal white adipose tissue samples were homogenized by a pellet pestle in ice cold lysis buffer. Briefly, all samples and standards

(50 ul each) were tested in duplicates, to which 25 μL of 1x HRP-cAMP was added. The plates were incubated at room temperature for 2 hours and after the washing steps, 100 μL of AbRed indicator was added. The plates were incubated for 1 hour and the fluorescence was measured at Ex/Em = 540/590 nm using a Biotek Synergy4 microplate reader.

Western Blotting

Western blots were performed using standard protocols. Adipose tissue lysates were made in NP40 lysis buffer: 150 mM NaCl, 1% NP40, 50 mM Tris 8.0 with phosphatase inhibitors. Lysates were prepared by sonication and the lysates were separated from overlaying fat layer by three rounds of centrifugation. After BCA method of protein quantification, lysates were boiled in Laemmli sample buffer (4% SDS, 20% glycerol, 10% 2-mercaptoethanol, 0.004% bromophenol blue and 0.125 M Tris HCl, pH 6.8). Blots were incubated with OxPhos antibodies (Thermofisher 45-8099 1:1000) and UCP-1 (Abcam ab10983). HRP-conjugated secondary antibodies were used at 1:5000 dilution and detected by enhanced chemiluminescence (ThermoFisher Scientific).

Glycerol Assay

Glycerol assays were performed using free glycerol detection reagent (Sigma, F6428) as per manufacturer's instructions. For serum glycerol, terminal blood collections were performed using cardiac puncture method and sera were frozen immediately at −80C until use. For glycerol detection, 1:20 ratio of sera to free glycerol reagent was used to perform the assay.

For *in vitro* differentiated adipocytes, wild-type and Opn3 null cells were dark adapted overnight on Day13 or Day14 of differentiation and serum starved for at least 3 hours on the day of the experiment. All cells were given fresh serum-free media before stimulating one set of wild- type and Opn3 null cells with blue light, while another set of cells were left in the dark incubator. Culture media was collected at the end of 2 hours of incubation in blue light or darkness and frozen on dry ice immediately for storage at −80C until use. For the glycerol assay, a 1:10 ratio of culture media to free glycerol reagent was used to determine the amount of glycerol released during the 2 hours of darkness or blue light stimulation.

Microarray Analysis

Interscapular adipose tissue complex and inguinal white adipose tissue from P16 mice were harvested at one hour after lights on (ZT1) and snap frozen on dry ice. Tissue pieces were homogenized in TRIzol (TriReagent Invitrogen) using RNase-free Zirconium oxide beads (2.0 mm) in a TissueLyser II (QIAGEN). Phase separation was achieved using chloroform and RNA in the aqueous phase was precipitated using ethanol. RNA was purified by column method using GeneJET RNA purification kit (ThermoFisher Scientific #K0732) and eluted into RNase-free water. RNA quality was assessed using the Agilent 2100 Bioanalyzer and an RNA-integrity number cut-off of 7 was applied for selecting samples for microarray assay. RNA from biological triplicates were submitted for microarray assay (ClariomD, Affymetrix) to the Technology Center for Genomics and Bioinformatics, University of California, Los Angeles.

Data analysis including normalization, gene expression changes and gene-enrichment analysis was performed using AltAnalyze, developed by Nathan Salomonis at Cincinnati Children's Hospital Medical Center. AltAnalyze uses the robust multi-array average method of normalization. Briefly, the raw intensity values are background corrected, log2 transformed and then quantile normalized. Next, a linear model is fit to the normalized data to obtain an expression measure for each probe set on each array. Gene expression changes greater than 1.1 fold were calculated using unpaired t test, where a p value < 0.05 was used as a cut-off.

Quantitative RT-PCR

Intrascapular adipose depots were harvested immediately following cold challenge assays. Snap frozen tissue was homogenized and processed for RNA as described above. RNA was treated with RNase-free DNase I (ThermoFisher Scientific #EN0521) and cDNA was synthesized using a Verso cDNA synthesis kit (ThermoFisher Scientific AB1453/B). Quantitative RT-PCR was performed with Radiant SYBR Green Lo-ROX qPCR mix (Alkali Scientific Inc.) in a ThermoFisher QuantStudio 6 Flex Real-Time PCR system. Primer information for quantitative PCR is included in the Table. Relative expression was calculated by the ΔΔCT method using *Tbp* (TATA binding protein) as the normalizing gene. Statistical significance was calculated by an unpaired t test, using a p value cut-off of < 0.05.

The primers used for the corresponding target gene are as follows:

Target	Forward primer	Reverse primer
Dio2	CAGTGTGGTGCACGTCTCCAATC	TGAACCAAAGTTGACCACCAG
Prdm16	CAGCACGGTGAAGCCATTC	GCGTGCATCCGCTTGTG
Pgc1a	CCCTGCCATTGTTAAGACC	TGCTGCTGTTCCTGTTTTC
Cidea	TGCTCTTCTGTATCGCCCAGT	GCCGTGTTAAGGAATCTGCTG
Ucp-1	ACTGCCACACCTCCAGTCATT	CTTTGCCTCACTCAGGATTGG
Pparγ	GTGCCAGTTTCGATCCGTAGA	GGCCAGCATCGTGTAGATGA
Hprt1	TCAGTCAACGGGGGACATAAA	GGGGCTGTACTGCTTAACCAG
Tbp	GAAGCTGCGGTACAATTCCAG	CCCCTTGTACCCTTCACCAAT

Transmission Electron Microscopy

Freshly dissected adipose tissues from P28 male mice were collected and 1 mm samples from approximately similar areas were fixed in 2% glutaraldehyde, 1% paraformaldehyde in PBS for 1 hour at room temperature before processing and sectioning for transmission electron microscopy as described before(Cinti et al., 2001).

NAD/NADH Quantification

NAD levels were measured using NAD/NADH assay kit from Abcam (ab65348). Briefly, tissues samples (inguinal adipose tissue and liver) from P16 mouse pups were snap frozen in liquid nitrogen, homogenized in NADH/NAD extraction buffer and filtered through a 10kD spin column (ab93349) to remove enzymes. Assay procedure was followed per kit instructions and levels of NADH and NAD+ were determined normalized to tissue weight.

Thermoregulation Assay

Core body temperature assessment upon acute cold exposure was performed on control and experimental male and female mice with the *Opn3* reporter null (*Opn3*$^{+/+}$ and *Opn3*$^{lacz/lacz}$), with the exon 2 deletion on the C57BL/6J background (*Opn3*$^{\Delta Ex2}$), with pan-adipocyte conditional deletion of *Opn3* (*Opn3*$^{fl/fl}$ and *Adipoq-cre; Opn3*$^{fl/fl}$), with brown adipocyte conditional deletion of *Opn3* (*Opn3*$^{fl/fl}$ and *Ucp1cre; Opn3*$^{fl/fl}$), with retinal conditional deletion of *Opn3* (*Opn3*$^{fl/fl}$ and *Rx-cre; Opn3*$^{fl/fl}$), and control and *Opn4* null mice. In addition, C57BL/6J mice reared under wavelength restriction (with or without blue, as described previously) were subject to this assay. Littermates were separated from their home cage and individually housed in a home-built lighting chamber situated in an electronically monitored 4°C cold room for 3 or 5 hours depending on the assay. While the mouse was conscious, body temperature was measured rectally with a RET-3 Microprobe Thermometer (Kent Scientific) every 20 minutes for the duration of the assay. Food and water were available *ad libitum* for all mice except when *Adipoq-cre; Opn3*$^{fl/fl}$ mice were fasted overnight, where food withdrawal was maintained during the cold assay. The thermo probe operator was blinded to mouse genotype and prior temperature measurements throughout the study. At the end of the cold exposure, mice were euthanized and relevant tissues were collected. The 3-hour cold exposure assays subjected mice to either a red (630 nm) and violet (380 nm) LED illumination combination (RV), or a red (630 nm), blue (480 nm) and violet (380 nm) LED combination (RBV). For the 5-hour cold exposure assays, the entirety of the 3-hour assay was extended by 2 hours following withdrawal of the 480 nm wavelength LED illumination. Two different ages of animals, postnatal day 21 (P21) and 2 month-old adults, were selected for these cold exposure assays. The order of cage placement was randomized at this time, such that the thermo probe operator remained blinded. For all cold exposure assays involving fed or overnight fasted *Adipoqcre; Opn3*$^{fl/fl}$ animals, intrascapular (iAT), inguinal (inWAT), and perigonadal (pgWAT) adipose tissues were harvested. Following animal euthanasia, the fat pads were manually dissected, and their weight recorded. For fat depots with left and right pads, both were harvested and weighed, and the average recorded per animal.

Indirect Calorimetry and Energy Expenditure

12–16-week-old *Opn3*$^{+/+}$ and *Opn3*$^{lacz/lacz}$ male mice were acclimated in metabolic chambers (PhenoMaster®, TSE Systems GmbH, Germany) for 3 days before the start of the study. Mice were continuously recorded for a total of 17 days with the following measurements taken every 15 minutes: gas exchange (O_2 and CO_2), food intake, water intake, and spontaneous locomotor activity (in the XY plane). Ambient temperature was adjusted via climate-controlled chambers that housed the metabolic chambers. VO_2, VCO_2, and energy expenditure (EE) were calculated according to the manufacturer's guidelines (PhenoMaster® Software, TSE Systems GmbH, Germany), with EE estimated via the abbreviated Weir formula. The respiratory exchange ratio (RER) was calculated by the ratio VCO_2/VO_2. Where appropriate, values were normalized by body weight (mL/hr/kg for VO_2 and VCO_2, and kcal/hr/kg for EE). Food and water intake were measured by top-fixed load cell sensors, from which food and water containers were suspended into the sealed cage environment. For food consumption, mice demonstrating excessive food grinding behavior were excluded from statistical analyses. After 9 days of continuous recording, cages were replaced with fresh ones and sealed, and gas exchange re-equilibration completed all within 2 hours.

Tail Infrared Thermography (FLIR)

Adult *Opn3*$^{fl/fl}$ and *Adipoq-cre; Opn3*$^{fl/fl}$ animals were placed in a tubular mouse restraint (Kent Scientific, Torrington, CT). These restraints permitted respiration via a slotted nose cone but immobilized the animal while exposing the tail through a rear port. IR thermographic images were taken with a FLIR T530 infrared camera (FLIR® Systems, Wilsonville, OR). Tail temperatures were quantified by describing a pixel-averaged circular region of interest of consistent size and rostrocaudal distance from the base of the tail.

QUANTIFICATION AND STATISTICAL ANALYSIS

Statistical analyses were performed using GraphPad Prism version 4.00 (GraphPad Software), Microsoft Excel and MATLAB 2018a (Figure 6). Two-tailed distribution, two-sample unequal variance *t*-test was used to determine the statistical significance between two

independent groups. Time series datasets between two groups (Figures 4, 5, and 6) were analyzed via one-way repeated-measures ANOVA. Datasets involving two or more factors (Figures 6G–6I) were analyzed by 2-way ANOVAs with Holm-Šídák corrected multiple comparisons.

DATA AND CODE AVAILABILITY

Whole-genome expression profiles are available at accession number GEO: GSE140757.